SECTION 3
MODEL VALIDATION AND ESTIMATION OF VARIABILITY

The essence of the validation process is calibrating any set of model parameters associated with a modeling method by limiting the misfit between the predicted and recorded motions. The residuals after optimization measure the inability of the method to predict the set of validation earthquake motions. In forward modeling exercises, following validation, the event-specific optimized parameters must be randomized to describe the range of parameter values that may occur in subsequent events.

The validation earthquake selected for the MCEER workshop is the 1988 Saguenay earthquake. It is the largest recorded ENA event and is documented by the most strong motion records of any ENA events. The exercise is to model the observed strong motions at nine stations on rock. Primarily, the validation is intended to assess to what extent each model predicts ground motions from a single previously recorded ENA earthquake. Because it also provides the participants the opportunity to calibrate individual model parameters, and insofar as these parameters are the basis for the subsequent scenario model estimates, the model calibrations enable each participant to provide the best possible estimates of ground motion.

Several of the models were previously validated against other earthquakes. These models should therefore be more finely tuned and capable of providing more robust ground motion estimates than those less well studied. Table 3-1 summarizes the number of validation earthquakes against which each model has been compared.

TABLE 3-1 Model Validation Summary

Modeler	Number of Earthquakes					Empirical Attenuation
	WUS	EUS	Subduction	Other	Total	
Anderson and Ni	5	1	0	3	9	No
Atkinson/Beresnev	1	1	2	0	4	Yes
Chiou	0	1	0	0	1	No
Hutchings and Jarpe	2	1	0	1	4	No
O'Connell	4	0	0	0	4	No
Silva	15	3	3	1	22	No
Somerville	6	4	4	0	14	No
Papageorgiou	6	2	0	0	8	No

Typically in validation studies, various source, path, or site parameters are prescribed that are based on results of independent studies of the validation earthquake. No such requirements were set forth in this study. Rather, the participants were allowed to calibrate any set of

parameters they deemed appropriate to the region and for the exercise. Discussion of model parameters was not a focus of the workshop.

3.1 Validation Earthquake

The scope of the workshop only allowed for a single validation earthquake. Two recent earthquakes were considered for use as the validation earthquake: the 1988 Saguenay, Ontario and the 1985 Nahanni, NW Territories events. The Saguenay event, an ENA earthquake, was well-recorded over a wide range of distances but its spectral content suggests that the mechanism may be anomalous compared to most other ENA and WUS earthquakes (see below). The Nahanni event has spectral content typical of ENA earthquakes but was recorded over an extremely limited distance range (about 8 to 16 km) and is not, technically, an ENA event. These limitations were judged to be significant enough that the Saguenay event was selected as the validation event.

The 25 November 1988 Saguenay earthquake was the largest to have occurred in ENA since the 1963 Baffin Bay event. The earthquake originated in the Grenville tectonic province of southern Quebec, in a relatively aseismic zone, with a nearly pure thrust mechanism (Somerville et al., 1990). The Saguenay event produced the largest set of strong motion records of any earthquake in the region: it was recorded at twelve sites within 200 km of the epicenter (Figure 3-1). Nine of the record sets from stations on rock sites were used in the validation studies (Table 3-2). Various magnitude estimates that describe the earthquake are (approximately): M_W 5.8, m_{bLg} 6.5, m_N 6.5 (short period magnitude), and m_b 5.9. The large discrepancy between m_{bLg}, m_N, and other scales was attributed to the spectral content of the source.

TABLE 3-2 Stations Used in Saguenay Validation Study

Station Number	Station Name	Distance (km)
S01	St-Ferreol	114
S02	Quebec	150
S05	Tadoussac	110
S08	La Malbaie	94
S09	St-Pascal	123
S10	Riviere-Ouelle	114
S16	Chicoutimi Nord	48
S17	St-Andre-du-Lac	66
S20	Les Eboulements	91

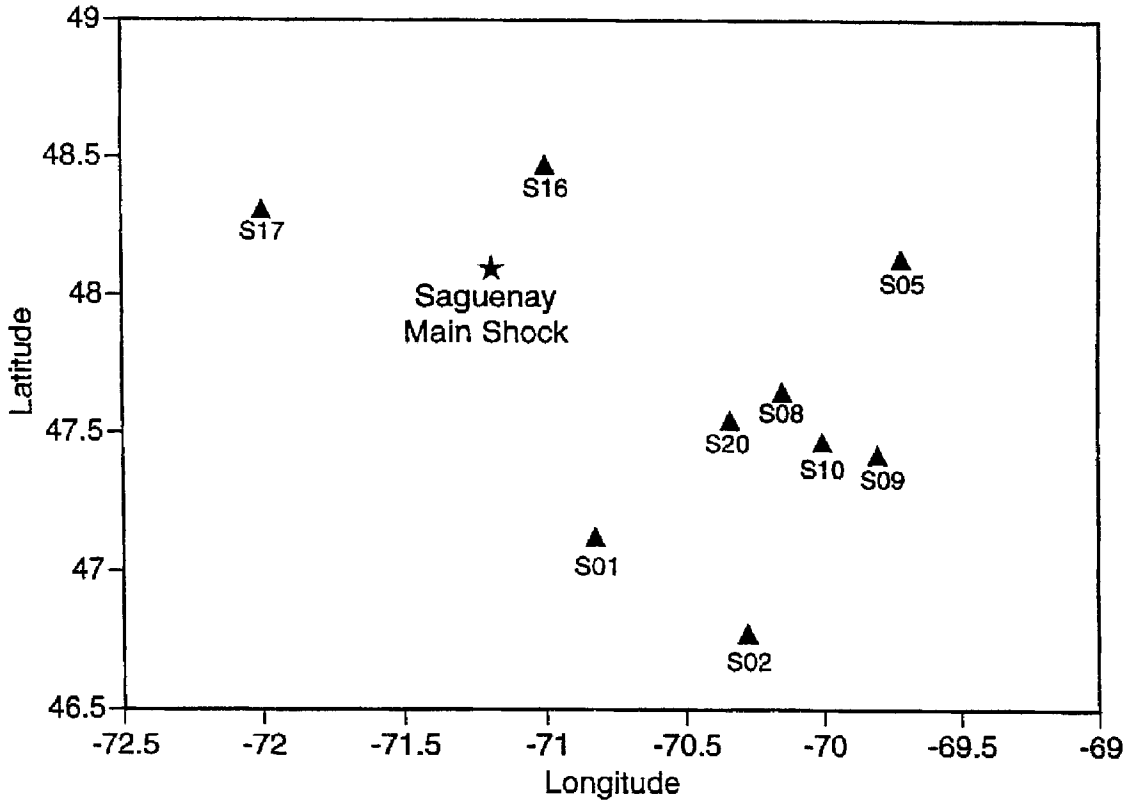

FIGURE 3-1 Saguenay Main Shock Epicenter and Strong Motion Recording Stations Used in Validation Exercises

This earthquake differed in two significant ways from other recent ENA events. Firstly, the focal depth, about 29 km, is notably deeper than most earthquakes in ENA which typically range from 5 to 15 km for larger events, causing critical reflections from the lower crust to occur at closer distances (Somerville et al., 1990). Only the 1968 Illinois event is known to have occurred at a similar depth. The centroid depth of about 26 km is based on an analysis of depth phases from teleseisms (Somerville et al., 1990) and is consistent with the deep hypocenter. Secondly, the high-frequency motion radiated from the source was exceptionally high and resulted in the over 0.5 magnitude unit difference between high frequency and other magnitude measures. The rich high-frequency content was not evident in other large earthquakes in the Saguenay sequence. Source studies have found that the main shock source was, in fact, not consistent with a single ω^{-2} source model (Boatwright and Choy, 1992). Haddon (1992) modeled the recorded motions with a unilateral rupture and short rise-times and concluded that these factors could account for the high-frequency content and Brune-scaling anomalies. However, Hartzell et al. (1994) derived a source model that consists mainly of a single compact asperity having a peak displacement of 2.6 m (high stress drop), which may account for the large ground motions. Lastly, ground motion levels significantly exceed those predicted using ENA attenuation relations within distances of about 120 km (Boore and Atkinson, 1992). This may be accounted for by the strong asperity, the large high-frequency energy radiated, unilateral rupture, or crustal characteristics resulting in a large "Moho bounce."

3.2 Results of Validation Exercise

The validation procedure involves optimizing any event-specific model and with the recorded ground motions. The validation process should include comparisons for a large number of earthquakes to evaluate the mean bias and modeling variability of the methods, however, for this exercise, we have only used one event to demonstrate the procedure. The strengths of the modeling methods should not be judges solely on the validation exercise from this one event.

In this study, the validation exercise using the Saguenay event was conducted for five of the models - Anderson/Ni, Atkinson/Beresnev (generic), Chiou, Hutchings and Silva. Somerville had validated his had validated his model previously (Somerville et al., 1990). Atkinson/Beresnev had also validated their stochasitc finite-fault model to the Saguenay earthquake as well as a WNA event and two subduction earthquakes (Beresnev and Atkinson, 1997, 1998b, 1998c). For the purposes of this study, they applied a generic ENA model and not one optimized for the Saguenay event. Both are generic and the optimized Saguenay validations for Atkinson/Beresnev are included.

Table 3-3: Summary of Realizations Performed in Saguenay Validation

Modeler	Number of Stations	Components			
		Horizontal H1	Horizontal H2	Average Horizontal	Vertical
Recorded Data	9	x	x		x
Anderson	9	x	x		x
Atkinson	9			x	
Chiou	9	x	x		x
Hutchings	9	x	x		x
Silva	9	x	x		

Recorded motions are compared to synthetics at all nine stations for the five models, in Appendix B. Included are seismograms (acceleration, velocity and displacement, horizontal and vertical), spectral acceleration (horizontal and vertical), and duration of motion (acceleration, velocity, and displacement; horizontal and vertical). Acceleration and velocity time histories for the two closest stations (16 and 17, at Chicoutimi Nord and St-Andre-du-Lac) are shown in Figures 3-2 and 3-3. Similar plots for two of the more distant stations (1 and 8, at St-Ferreol and La Malbaie) are shown in Figures 3-4 and 3-5. Most of the predictions give a reasonable agreement to the shape of the recorded time history during the strongest shaking, but the amplitudes can vary by a factor of 4 in peak ground acceleration (PGA). The response spectra of the predicted and recorded ground motions for these four stations are compared in Figure 3-6. At individual frequencies, the response spectra from the various model predictions vary by factors of 3 to 10.

The acceleration duration of the predicted and recorded ground motions for the four stations are compared in Figure 3-7. The duration is defined using the normalized Arias intensity. The duration is the time interval between 5% and 100x% of the arias intensity. For example, the time interval between 5% and 90% of the arias intensity is plotted at x=0.9. Similarly, the time interval between the 5% and 50% arias intensity is plotted at x=0.50. These plots indicate how the energy is distributed through time in the ground motion. The alternative simulation procedures vary in duration by a factor of 5 to 10.

The horizontal spectral acceleration residuals for the nine Saguenay stations are shown on the left hand side of Figure 3-8 for the individual simulation models. The standard deviation of the residuals is shown on the left hand site of this figure. The average residual computed from all nine Saguenay stations for the models are compared in the top frame of Figure 3-9a. The lower frame compares the standard deviation of the residuals. There is no consistent trend of over- or under-prediction with frequency for all of the models. Overall, the Anderson/Ni model shows the least bias at all periods. The modeling variability similarly shows no single trend with period; they are generally between about 0.6 and 1.0 natural log units.

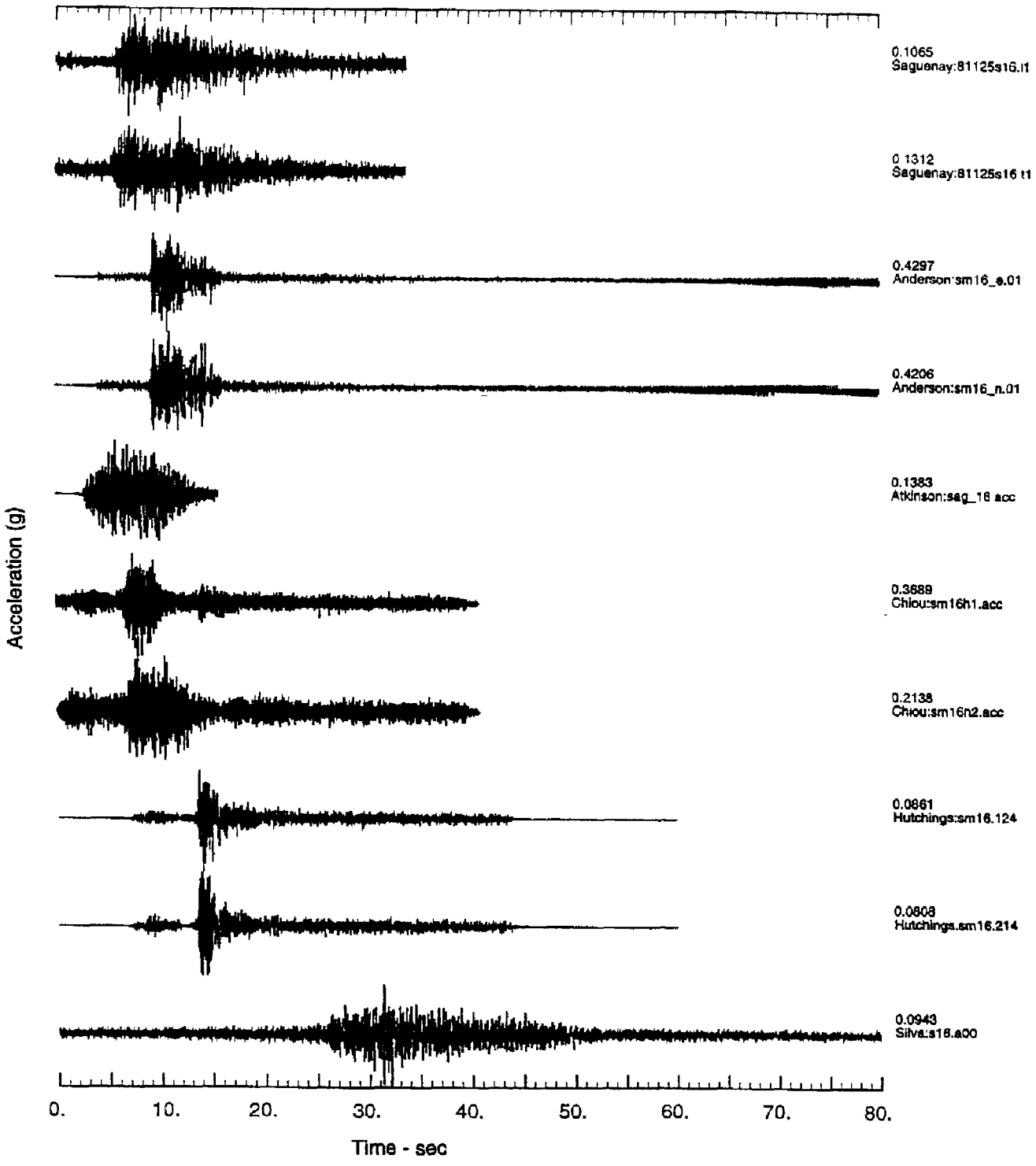

FIGURE 3-2a Comparisons of Recorded Chicoutimi Nord Accelerations and Validation Synthetics, Horizontal Components

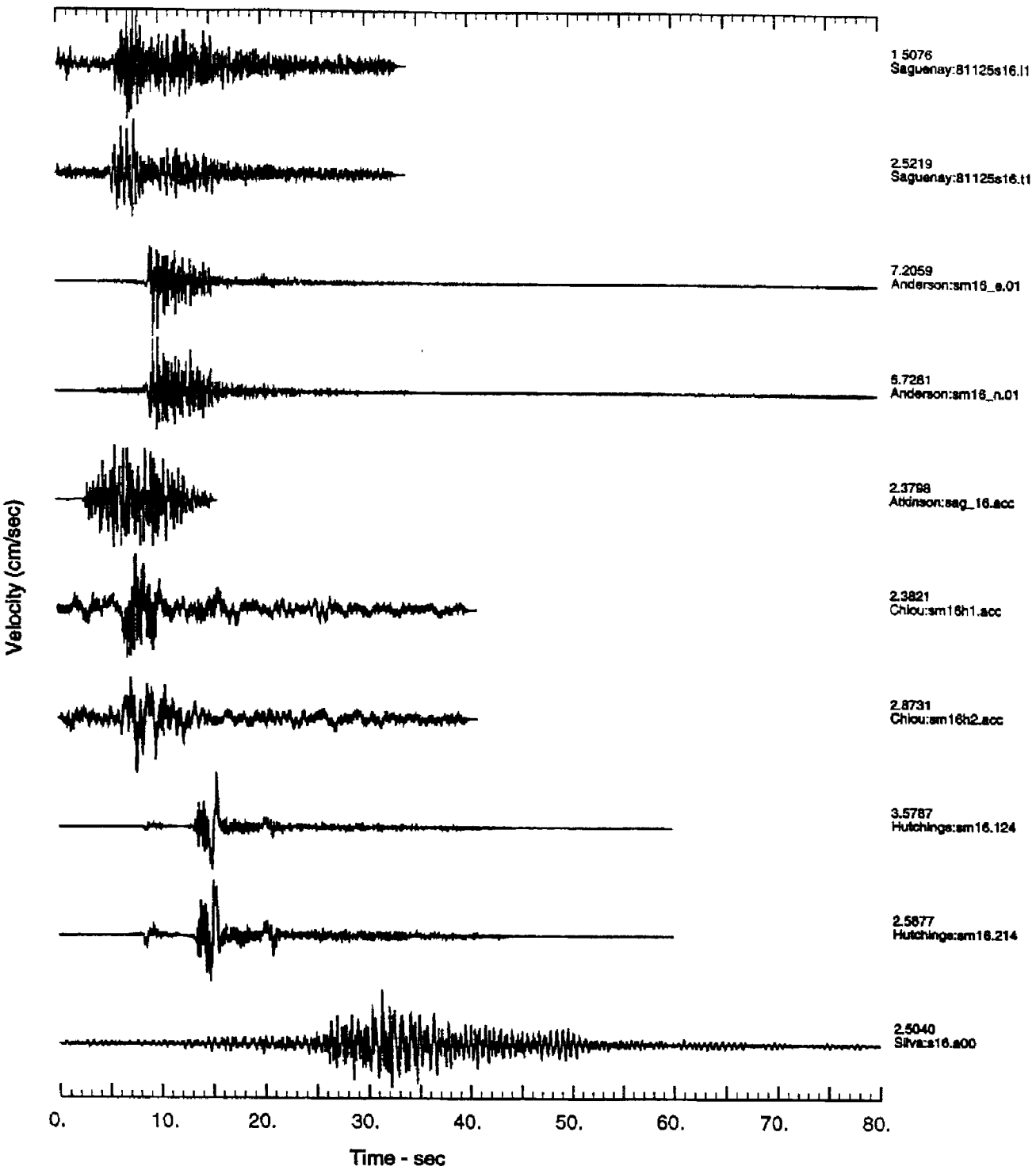

FIGURE 3-2b Saguenay Validations, Horizontal Velocity Components: Chicoutimi Nord

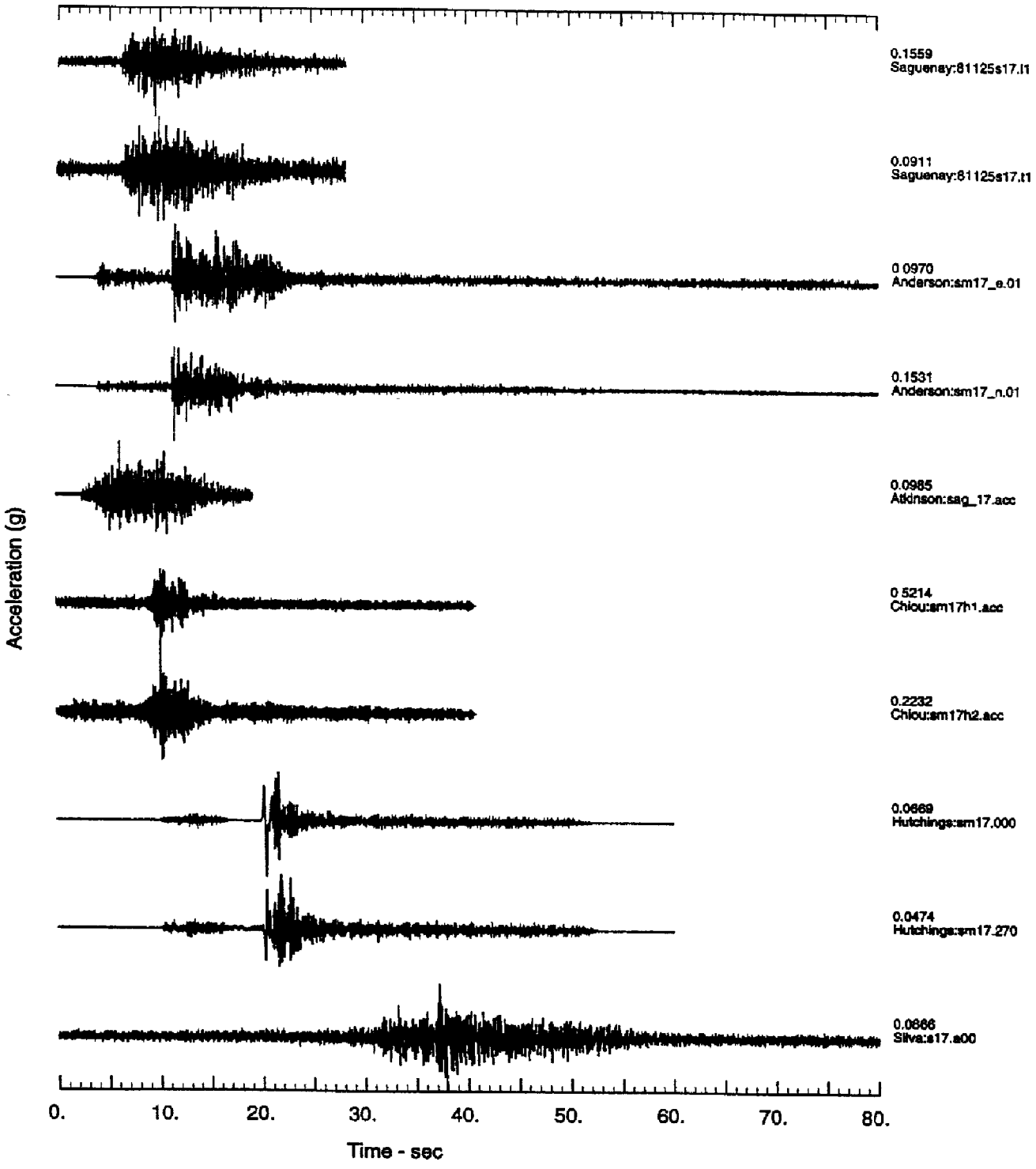

FIGURE 3-3a Comparisons of Recorded St-Andre-Du-Lac Accelerations and Validation Synthetics, Horizontal Components

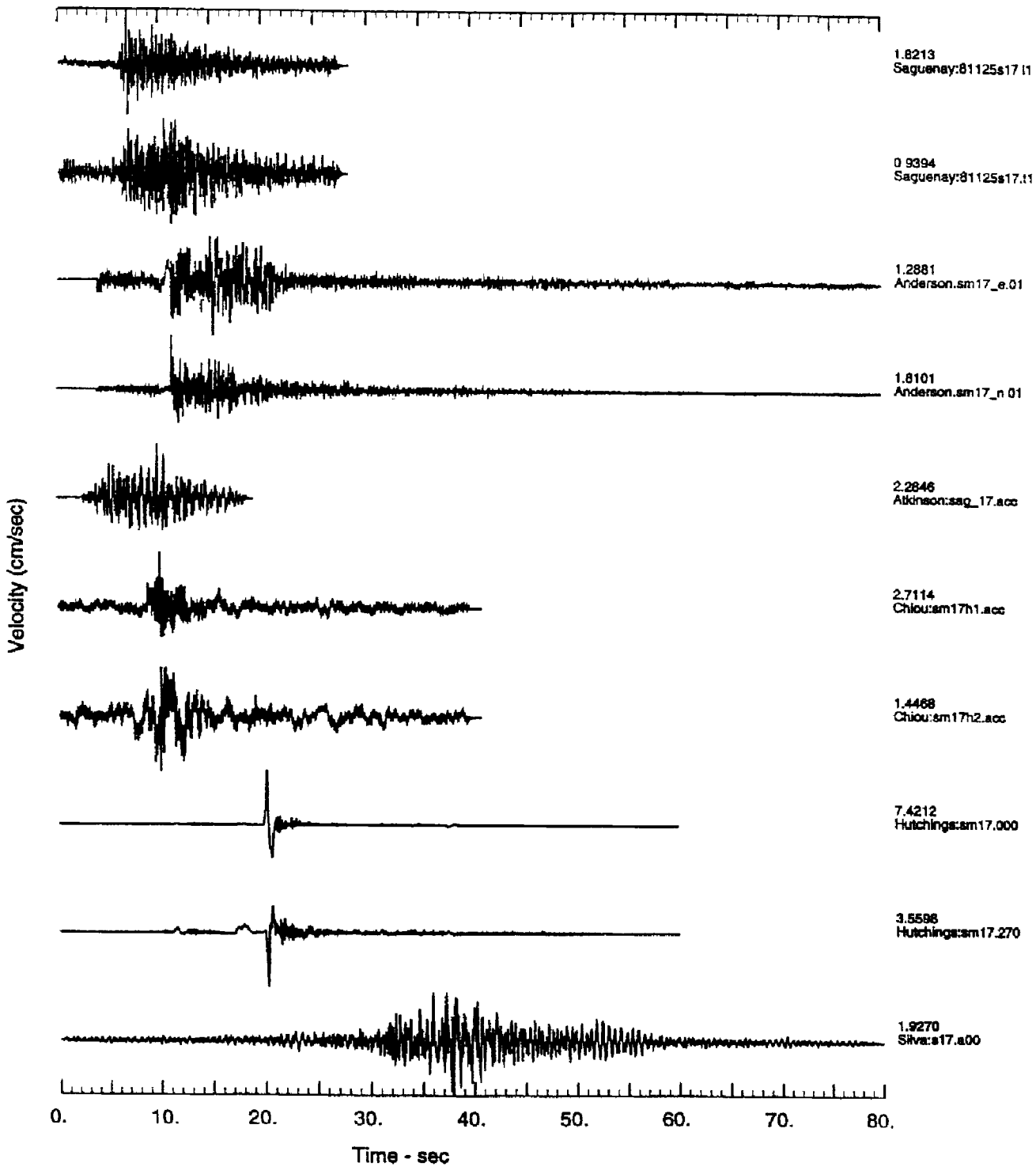

FIGURE 3-3b Saguenay Validations, Horizontal Velocity Components: St-Andre-Du-Lac

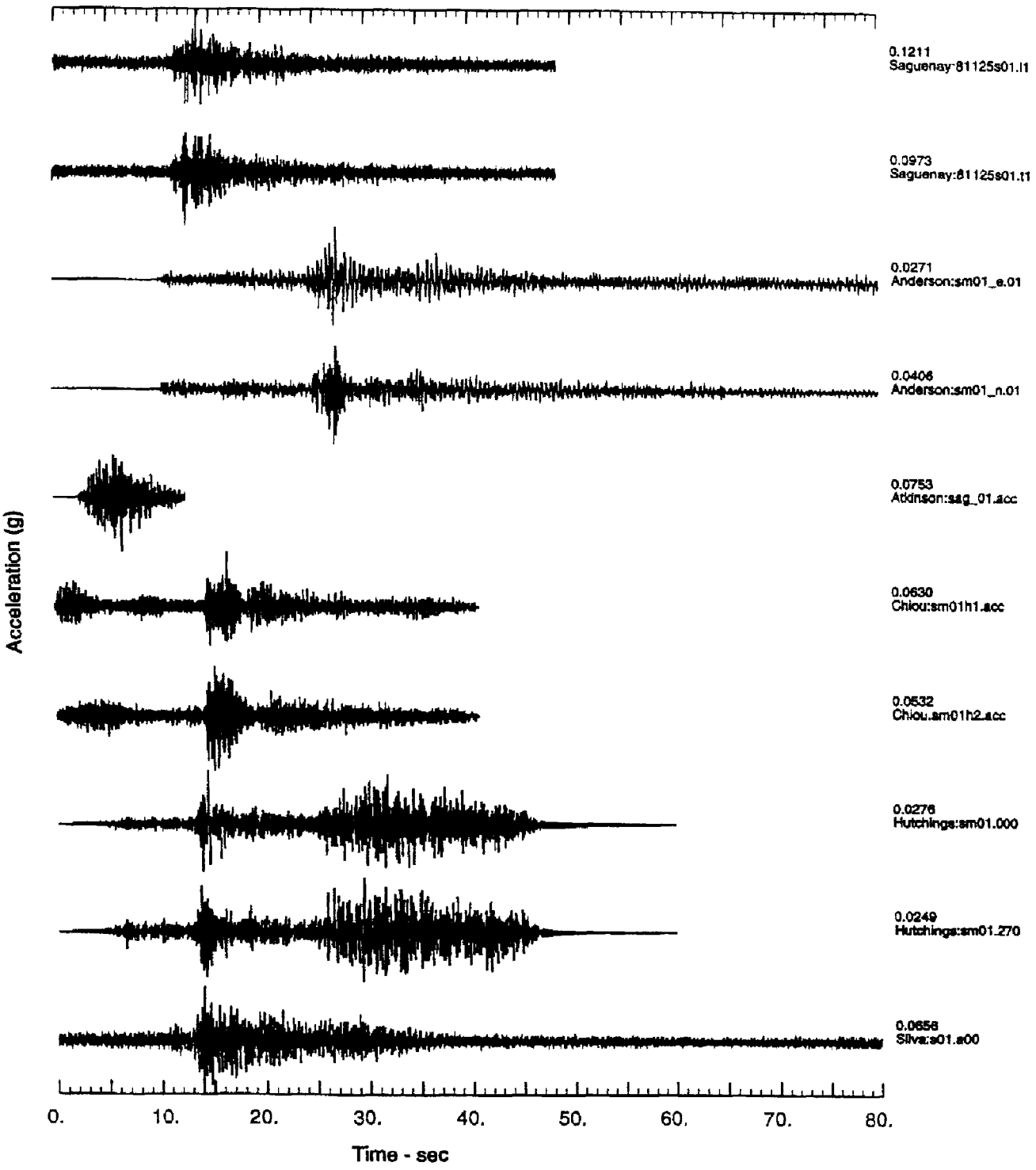

FIGURE 3-4a Comparisons of Recorded St-Ferreol Accelerations and Validation Synthetics, Horizontal Components

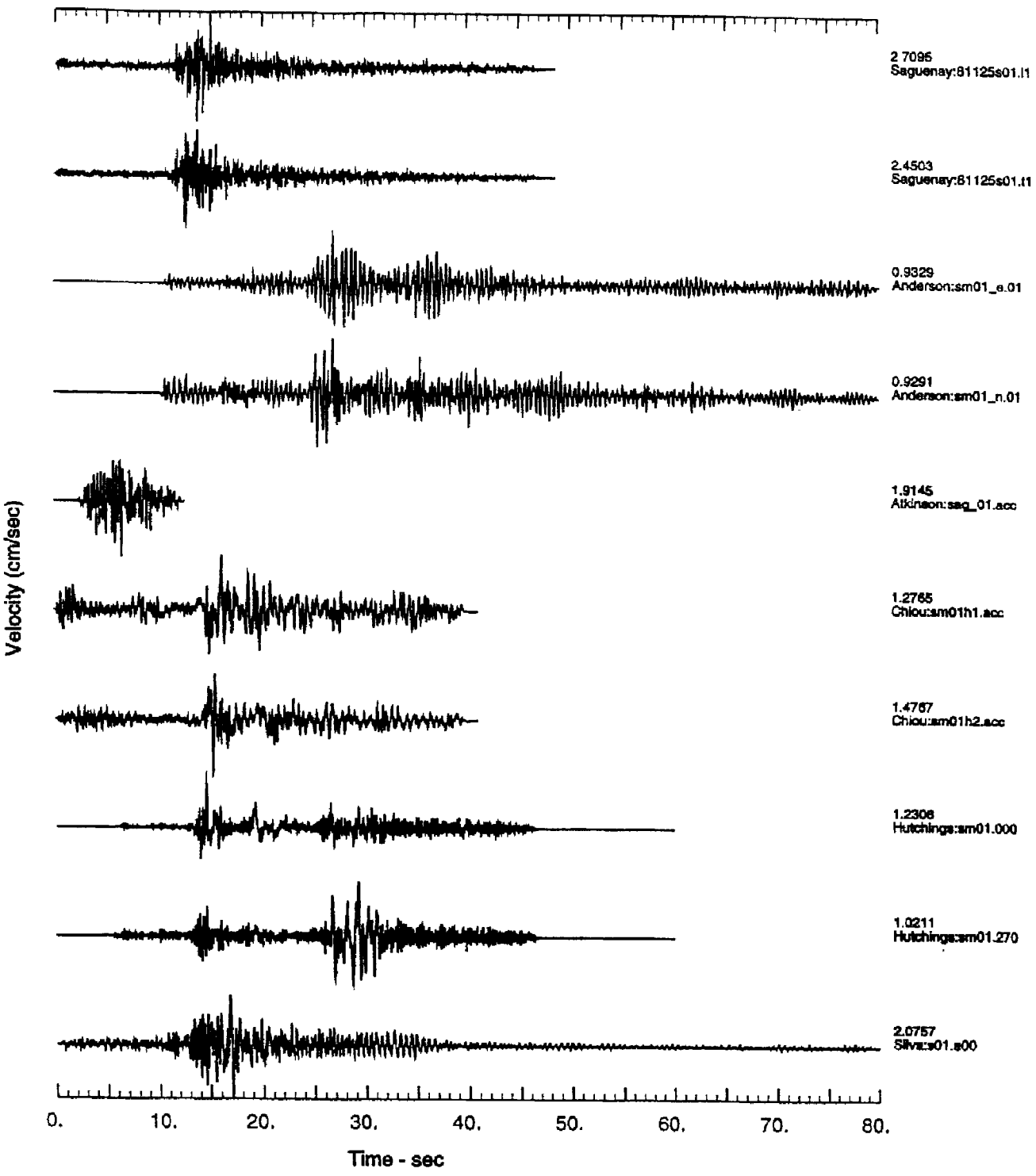

FIGURE 3-4b Saguenay Validations, Horizontal Velocity Components: St-Ferreol

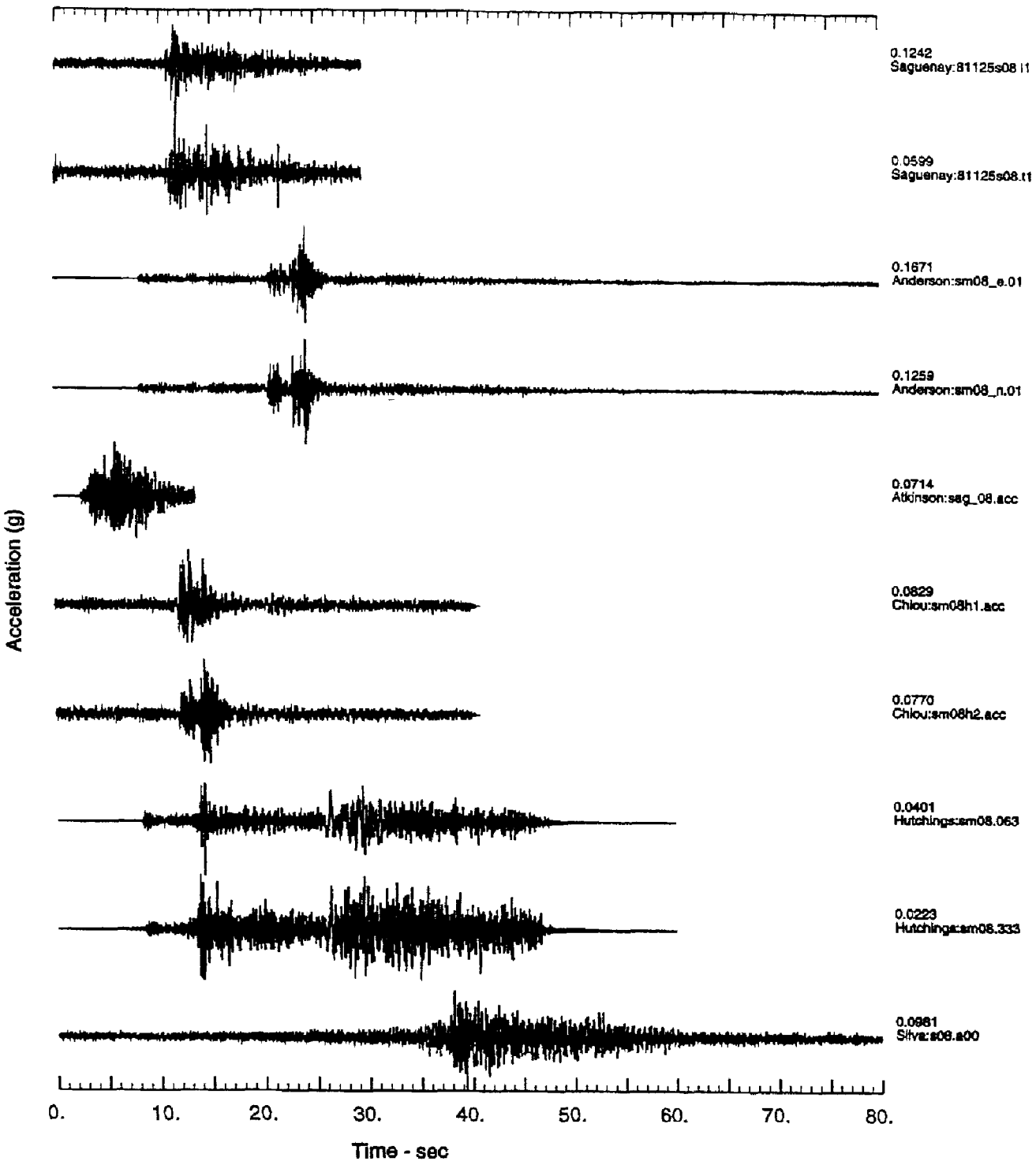

FIGURE 3-5a Comparisons of Recorded La Malbaie Accelerations and Validation Synthetics, Horizontal Components

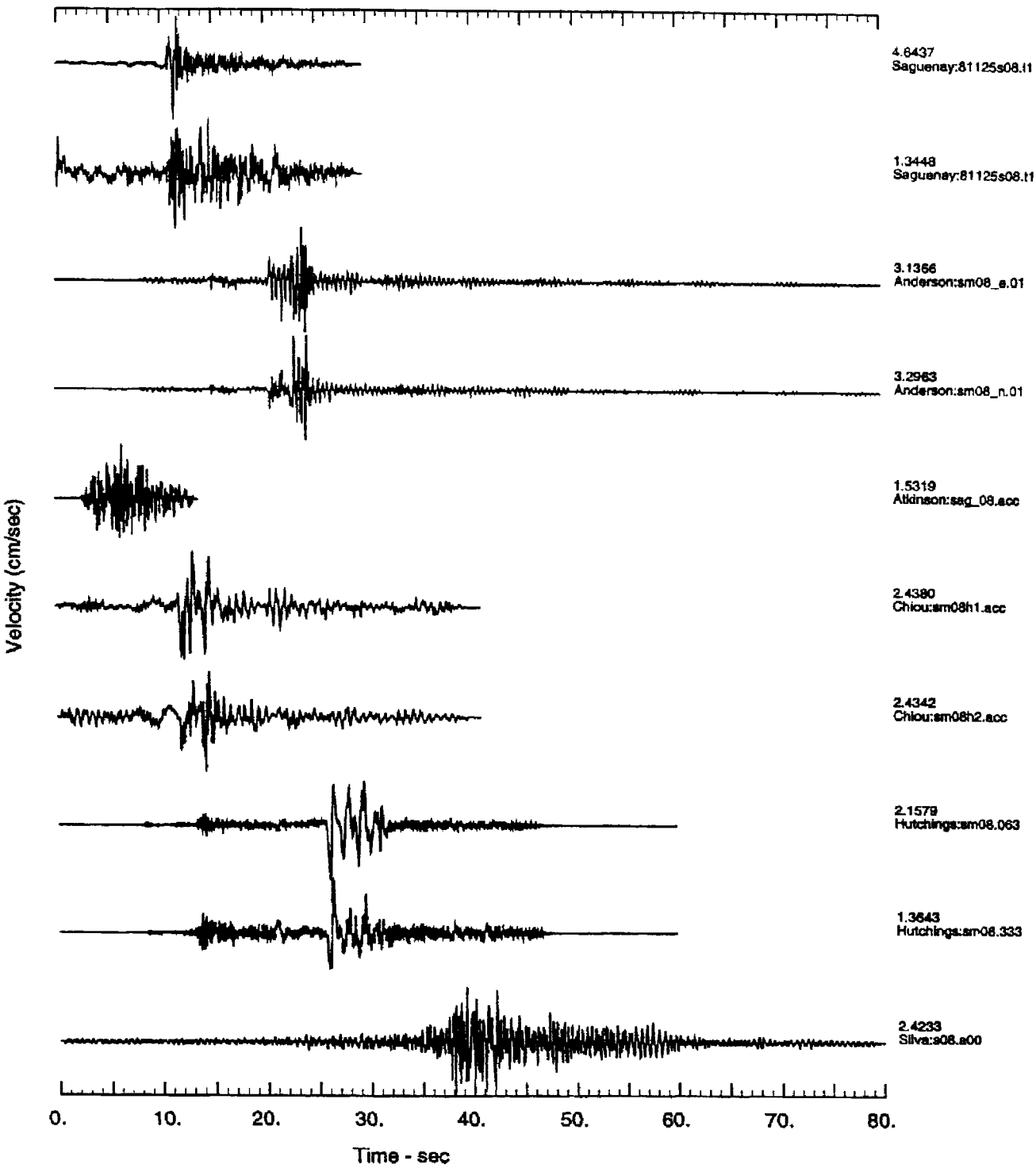

FIGURE 3-5b Saguenay Validations, Horizontal Velocity Components: La Malbaie

The mean residual and modeling variability shown in Figure 3-9a is for only one earthquake. This is not an adequate data set on which to develop robust model bias and modeling variability estimates. Some of the simulation methods had been previously validated against a larger number of earthquakes. Anderson/Ni, Silva, Somerville, and Atkinson/Beresnev each have previously computed model bias using several EUS and WUS earthquakes. The model bias and modeling variability for these more extensive validations are shown in Figure 3-9b. For these more extensive validations, the model bias and modeling variability are much smaller at high frequencies than for the Saguenay validation by itself.

The residuals for acceleration duration for the Saguenay validation are shown in Figure 3-10. The Anderson/Ni model shows the least bias over all intensity intervals. The Atkinson/Beresnev model tends to underpredict the acceleration duration whereas the Chiou, Hutchings and Silva models tend to overpredict the acceleration duration.

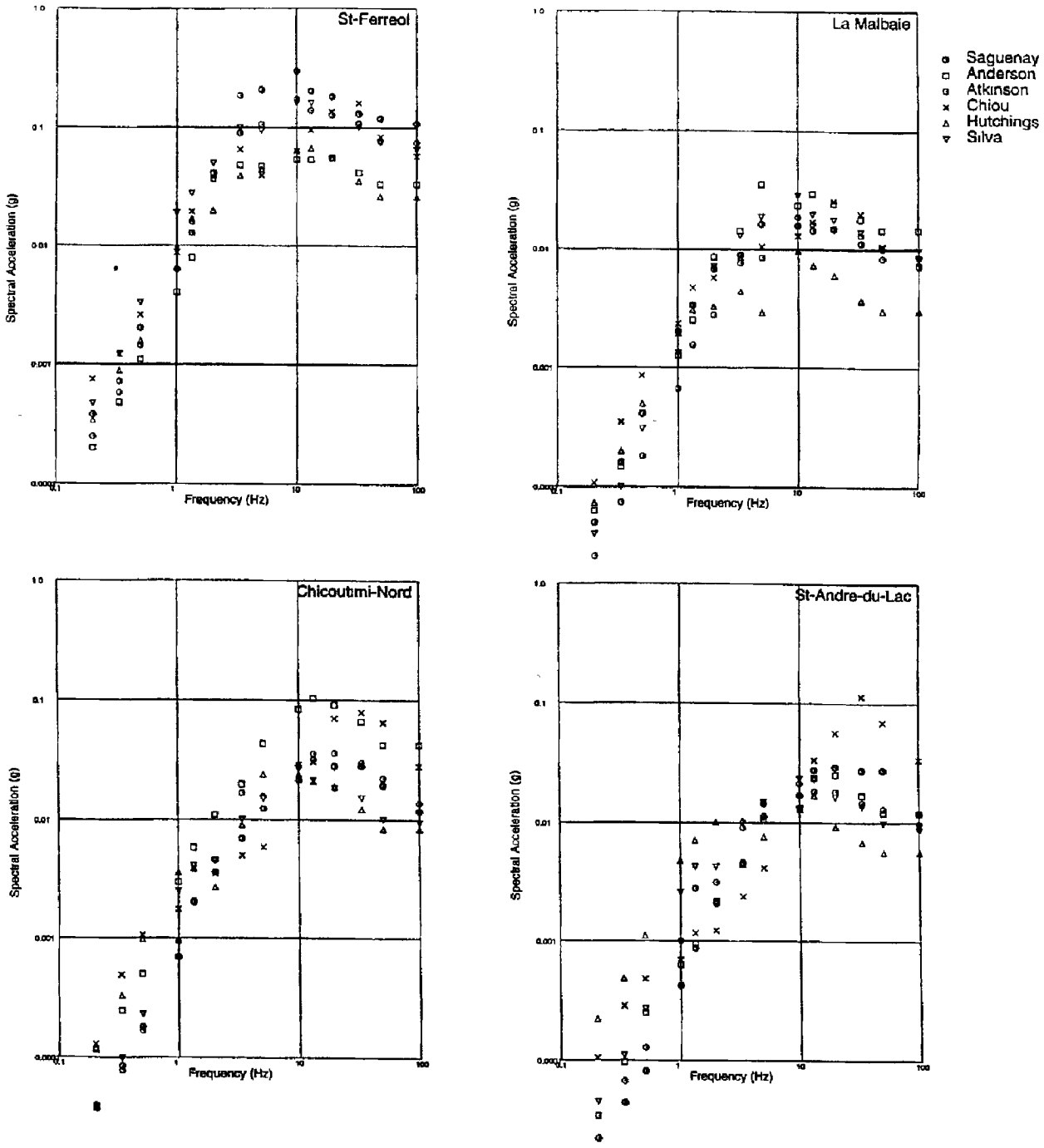

FIGURE 3-6 Spectra Comparisons for Saguenay Recordings and Validation Synthetics, Horizontal Component, 5% Damping

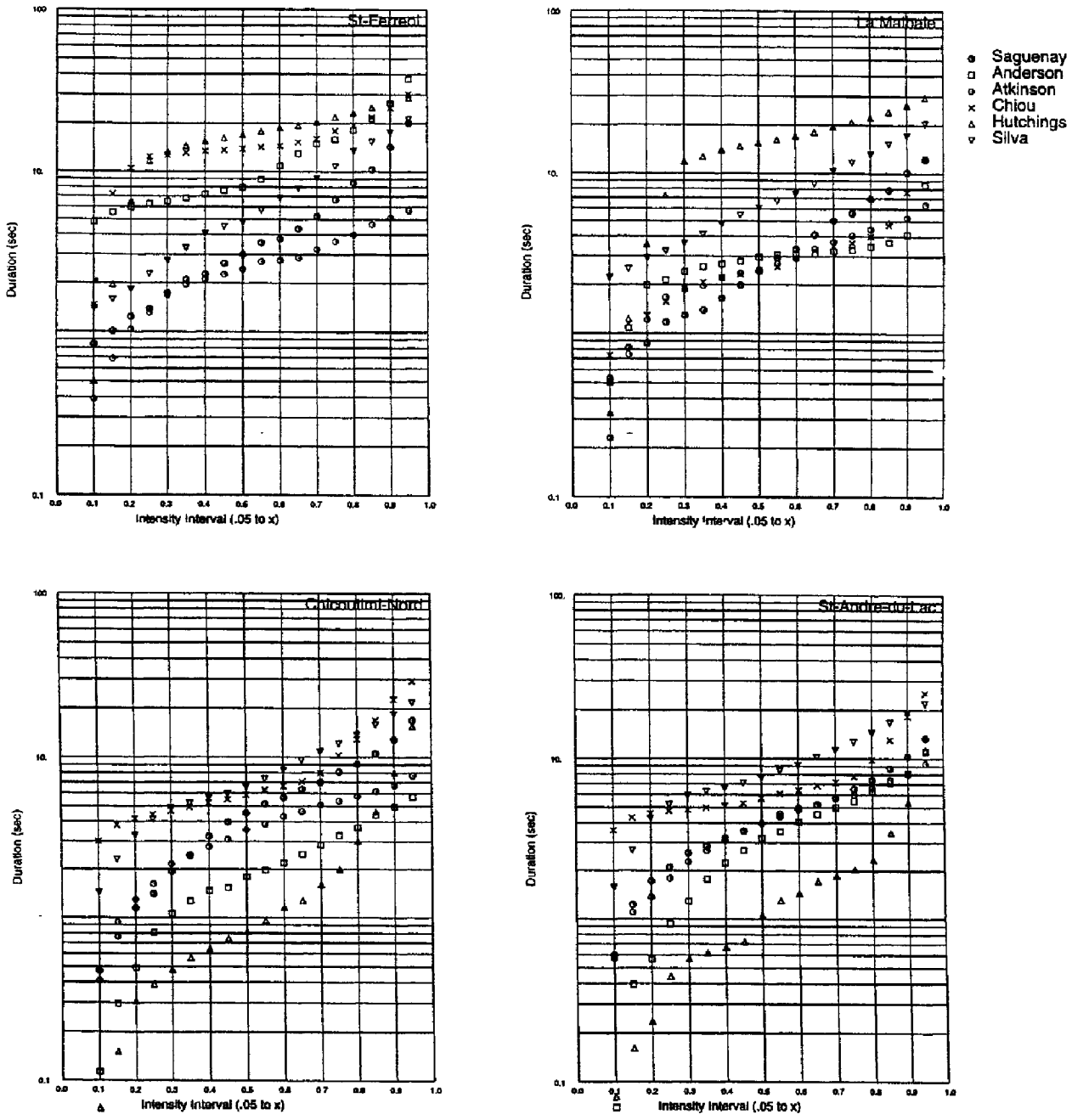

FIGURE 3-7 Comparison of Acceleration Durations Computed for Saguenay Records and Validation Synthetics, Horizontal Component

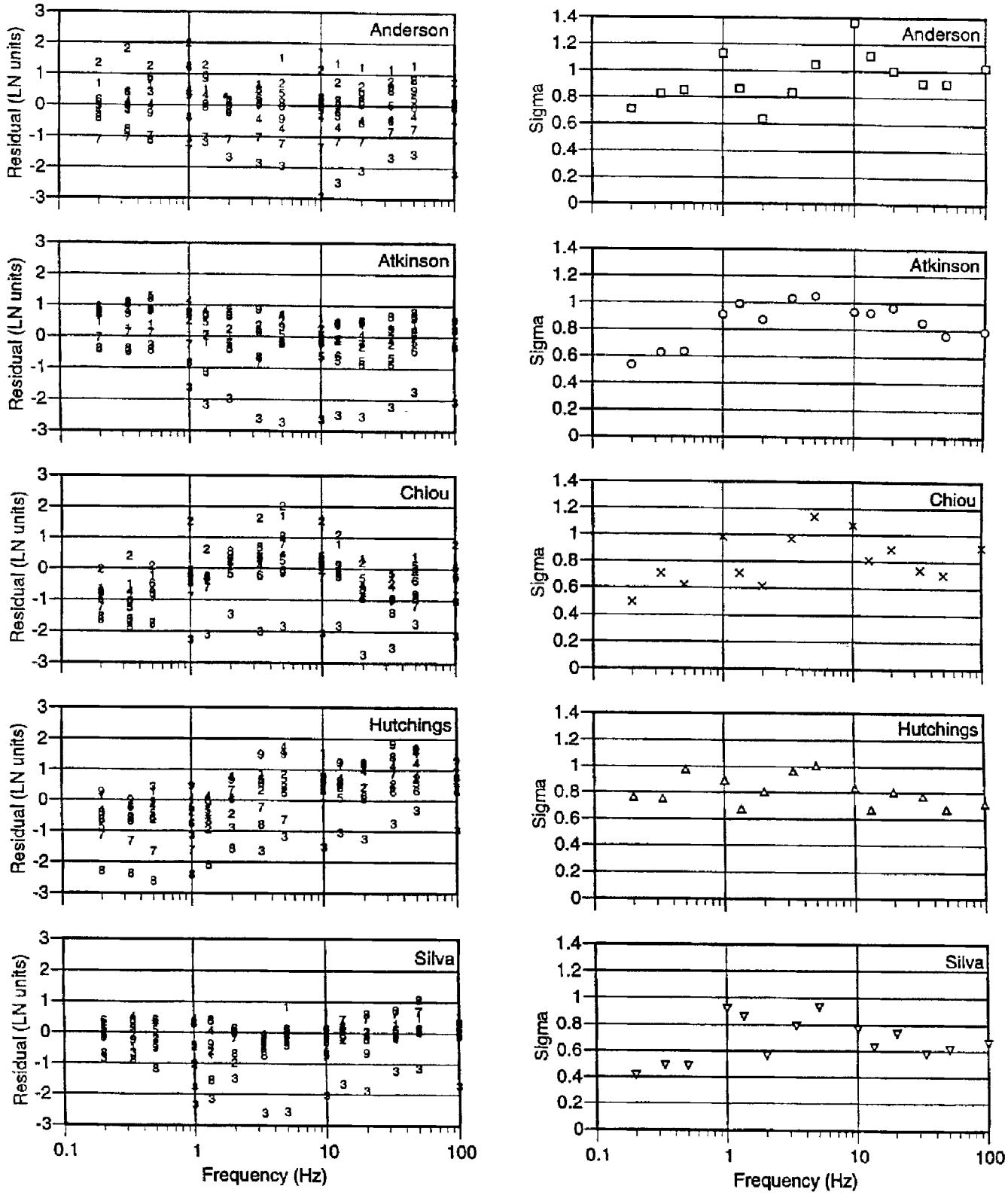

FIGURE 3-8 Residuals of Horizontal Spectral Acceleration for the Nine Saguenay Stations

(Note: A positive model bias reflects underprediction, negative reflects overprediction. Residuals at each recording site are indicated by the order listed in Table 3-2.)

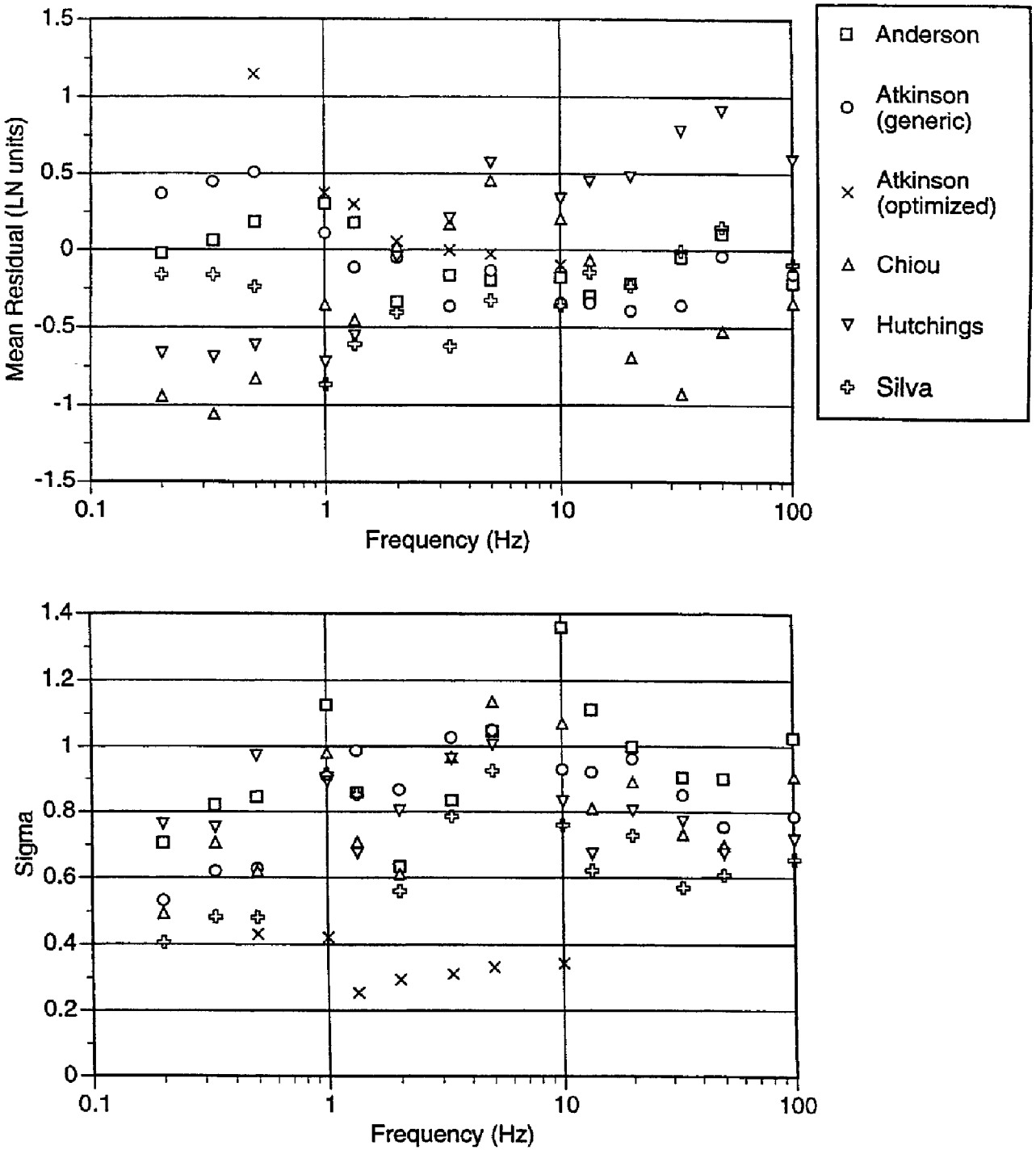

FIGURE 3-9a Model Bias and Modeling Variability Based on the Saguenay Earthquake Only (Average Horizontal Acceleration)
(Note: A positive model bias reflects underprediction, negative reflects overprediction.)

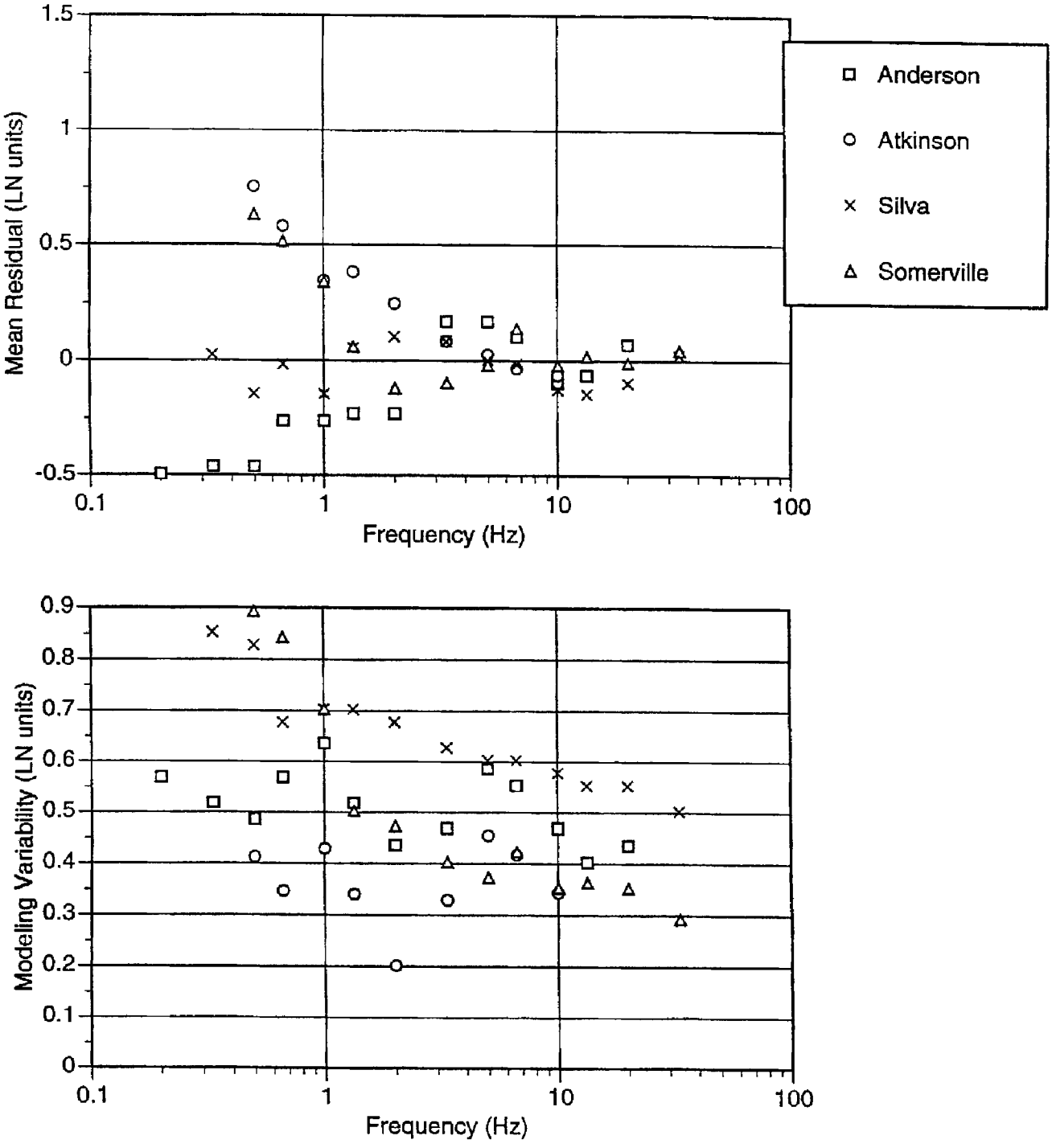

FIGURE 3-9b Model Bias and Modeling Variability Based on Various Other Validation Studies
(Note: A positive model bias reflects underprediction, negative reflects overprediction.)

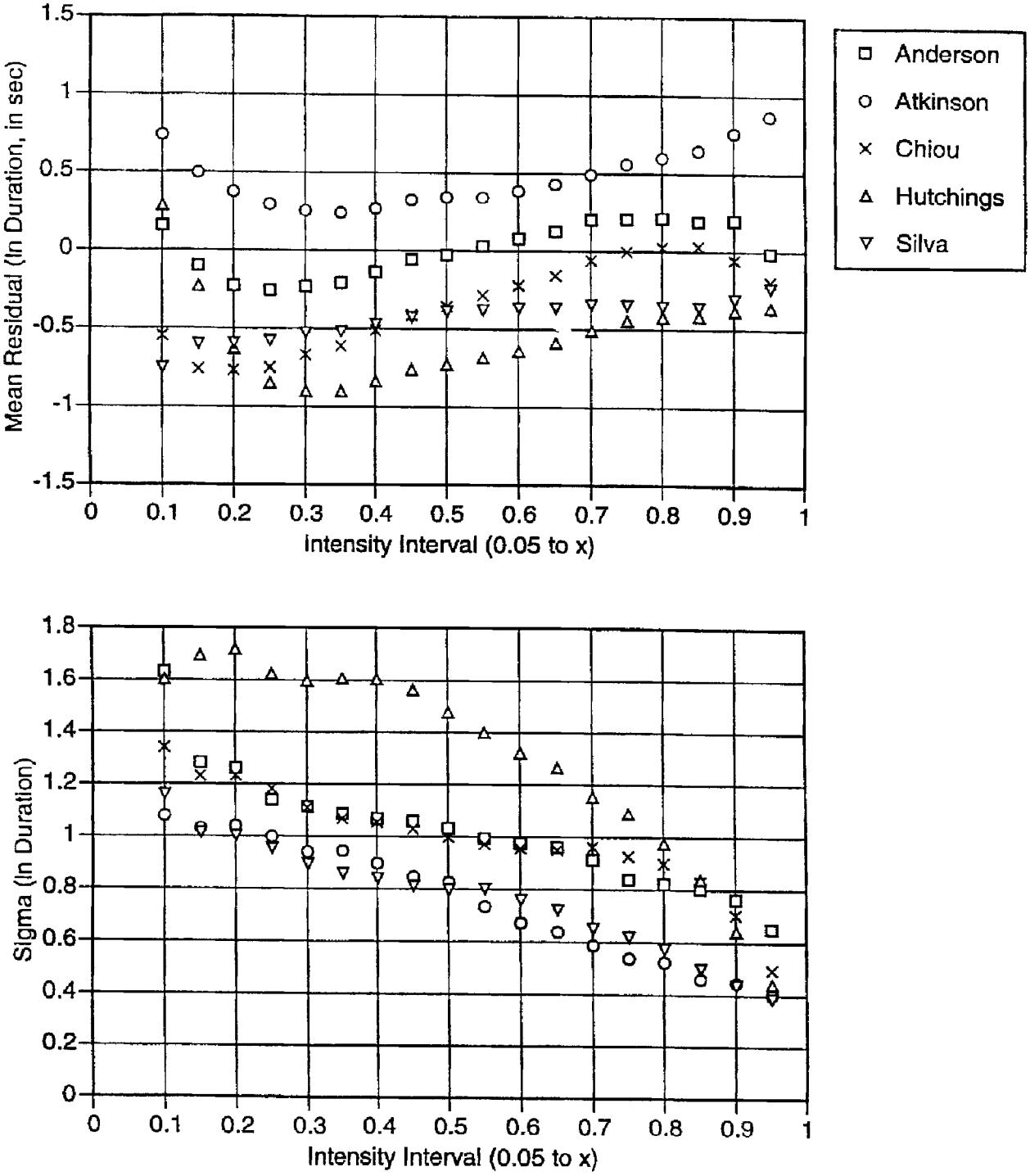

FIGURE 3-10 Model Bias and Modeling Variability Based on the Saguenay Earthquake Only (Horizontal Acceleration Duration)
(Note: A positive model bias reflects underprediction, negative reflects overprediction.)

SECTION 4
SCENARIO EVENT GROUND MOTIONS

In forward modeling of a scenario event, a fault geometry and select source, path, and site parameters are typically specified. Parameters not specified, including details of the rupture process and parameters optimized in the validation, are randomized to model the range of their uncertainty in future events.

In this study, fault geometry, event magnitude, event rake, velocity structure, and site kappa were all specified (Table 4-1). The scenario earthquake adopted for this study is a thrust event with moment magnitude 7.0 occurring on a 45° east-dipping plane. The fault dimensions are 50 km long and 20 km wide. The top of the rupture zone lies 2 km below the ground surface thus precluding energy release in the very near-surface. The EPRI Mid-continent crustal velocity model (Fig. 4-1) and Q-model were stipulated. Simulations were performed at a suite of 30 sites surrounding a dipping fault plane (Table 4-2, Fig. 4-2). All sites are hard rock.

Table 4-1a: Scenario Event Source Parameters

Magnitude	7.0
Event Rake	90°
Fault Dip	45°
Site Kappa	0.006
Q	$670 f^{0.33}$

Table 4-1b: EPRI Mid-Continent Crustal Model

Layer Thickness (km)	Depth to Layer Top (km)	V_P (km/sec)	V_S (km/sec)	Density (gm/cc)
1	0	4.9	2.83	2.52
11	1	6.1	3.52	2.71
28	12	6.5	3.75	2.78
-	40	8.0	4.62	3.35

The approaches adopted to represent source, path, and site effects are summarized in Table 4-3 for each participant. Each of the source parameters that were optimized in the validation exercise was to be varied in the simulations. These may have included slip model, hypocentral location, sub-event parameters, or any other parameters relevant to a specific model. Parameters that were randomized in the simulations by each participant are summarized in Table 4-4. A minimum of ten source realizations was suggested to define the parametric variability. Not all participants were able to provide a complete suite of synthetic motions, or

provide synthetics at each of the 30 sites. Motions that were provided are summarized in Table 4-5.

The output for the modeling exercise was standardized in order to facilitate comparisons of results. All ground motion estimates were provided as accelerations in g in a specified format. Three components of motion were requested, as appropriate for each model.

Table 4-2: Site Coordinates

Site	x-Dist (km)	y-Dist (km)
1	-10	5
2	5	5
3	10	5
4	25	5
5	50	5
6	80	5
7	100	5
8	120	5
9	150	5
10	200	5
11	300	5
12	500	5
13	-10	15
14	5	15
15	10	15
16	25	15
17	50	15
18	80	15
19	100	15
20	120	15
21	150	15
22	200	15
23	300	15
24	500	15
25	5	25
26	5	40
27	5	80
28	5	100
29	5	120
30	5	150

Table 4-3: Models for Source, Path, Scatterer and Site used in Scenario Realizations

Participant	Source	EUS[1] Source	Path	Scatterer	Site
Anderson/Ni	ω^2	$\Delta\sigma_{sub}$, $V_{rupture}$, R_{max}	FK, Q	Model	Q, kappa
Atkinson/ Beresnev	ω^2	RS^2 Factor, Sub-fault Size[3]	Empirical EUS	Empirical Duration	kappa
Chiou	ω^2	Rise Time	FK, Q	Model	kappa
O'Connell	Finite Fault	Variable local stress drop, rise times, and asperity positions	Rays	Empirical WUS[4]	Empirical WUS
Silva	ω^2		Rays, Q	Empirical EUS	kappa
Somerville	Finite Fault	Static $\Delta\sigma$	Green's Functions, Q	Empirical WUS	kappa
Hutchings/ Jarpe[5]	Kinematic		EUS Green's Function	EUS Green's Function	EUS Green's Function
Papageorgiou[5]	Circular Crack (Sub-event)	$\Delta\sigma_{Local}$ $\Delta\sigma_{Global}$	Green's Function	Scattered Wave Energy Model	Q (≈kappa)

Notes:

1 *Eastern U.S.*

2 *Fixed to Saguenay values*

3 *Radiation-strength factor*

4 *Western U.S.*

5 *Participant did not provide scenario motions; parameters shown reflect the model approach that would have been adopted*

Table 4-4: Parameters Randomized in Scenario Realizations

Participant	Randomized Parameters			Fixed Parameters[1]
	Hypocenter	Slip Distribution	Rise Time	
Anderson	x	x	x	$\Delta\sigma_{sub}$, R_{max} , $V_{rupture}$
Silva	x	x	x (Sub-event)	$\Delta\sigma_{sub}$, Mainshock Rise Time
Chiou	x	x	x	
Somerville	x	x	x	
Atkinson	x	x		RS Factor, Grid size
O'Connell	x	x	x	
Hutchings[2]	x	x	x	
Papageorgiou[2]	x	x		

Notes:

[1] *Parameters optimized in validation study*

[2] *Participant did not provide scenario motions; parameters shown are model approach that would have been adopted*

Table 4-5: Summary of Simulations Provided by Participants

Participant	Number of Stations[1]	Components Simulated				Number of Realizations Computed
		East	North	Average Horizontal	Vertical	
Anderson	26[2]	x	x		x	10
Atkinson	30			x		10
Chiou	25[3]	x	x		x	12
O'Connell	10[4]	x	x		x	800[5]
Silva	30			x		30
Somerville	26[6]	x	x		x	27

Notes:

[1] *30 possible*

[2] *Stations 11, 12, 23, and 24 were omitted.*

[3] *Stations 11, 12, 23, 24, and 30 were omitted.*

[4] *Stations modeled include 1, 2, 3, 4, 13, 14, 15, 16, 25, and 26.*

[5] *Ten slip models and the 1st, 21st, and 80th hypocenters generated by O'Connell were used (30 total).*

[6] *Stations 11, 12, 23, and 24 were omitted.*

4.1 Modeling Results

Each participant developed suites of synthetics at each of thirty sites surrounding the scenario rupture. All synthetics are shown in Appendices C through G for the six participants in the simulation exercise. Appendices H and I summarize the horizontal and vertical results as spectra and acceleration, velocity, and displacement duration. A sample of these results is reproduced as Fig. 4-3 through 4-20 at sites 1, 21, and 29. These are located on the footwall near the center of the rupture plane, 120 km normal to the strike of the plane on the hanging wall, and 150 km along-strike, respectively (Fig. 4-2).

The mean horizontal acceleration response spectra from the simulations are shown in Figures 4-3, 4-4, and 4-5 for the three sites. The horizontal spectra are all within a factor of 3-5 of each other for the close in site and the distant sites. The parametric variability is computed from each participants suite of realizations and is shown in the lower frame of Figures 4-3 to 4-5. The parametric variability is relatively small and ranges between about 0.1 to 0.4 (natural log units) at high frequencies and is slightly greater at low frequencies. This parametric variability is much smaller than the variability between mean model predictions.

The mean horizontal acceleration duration from the simulations is shown in Figures 4-6, 4-7, and 4-8 for the three sites. For the short distance site, four of the models produce similar durations: Anderson/Ni, Atkinson/Beresnev, Somerville, and Chiou. The Silva model produces much longer durations and the O'Connell model produces much shorter durations. For the two distant sites, the mean durations vary by about a factor of 2. The Anderson/Ni model, which includes scattering effects, produces the longest durations (Fig. 4-8). The parametric variability of the duration is shown in lower frame of Figures 4-6 to 4-8. For site 21, the parametric variability is very small (less than 0.2 natural log units) but for site 29, off the end of the fault, the parametric variability is much larger (0.1 to 0.6 natural log units). This increase in parametric variability is probably due to variable hypocenter locations leading to forward and backward directivity conditions.

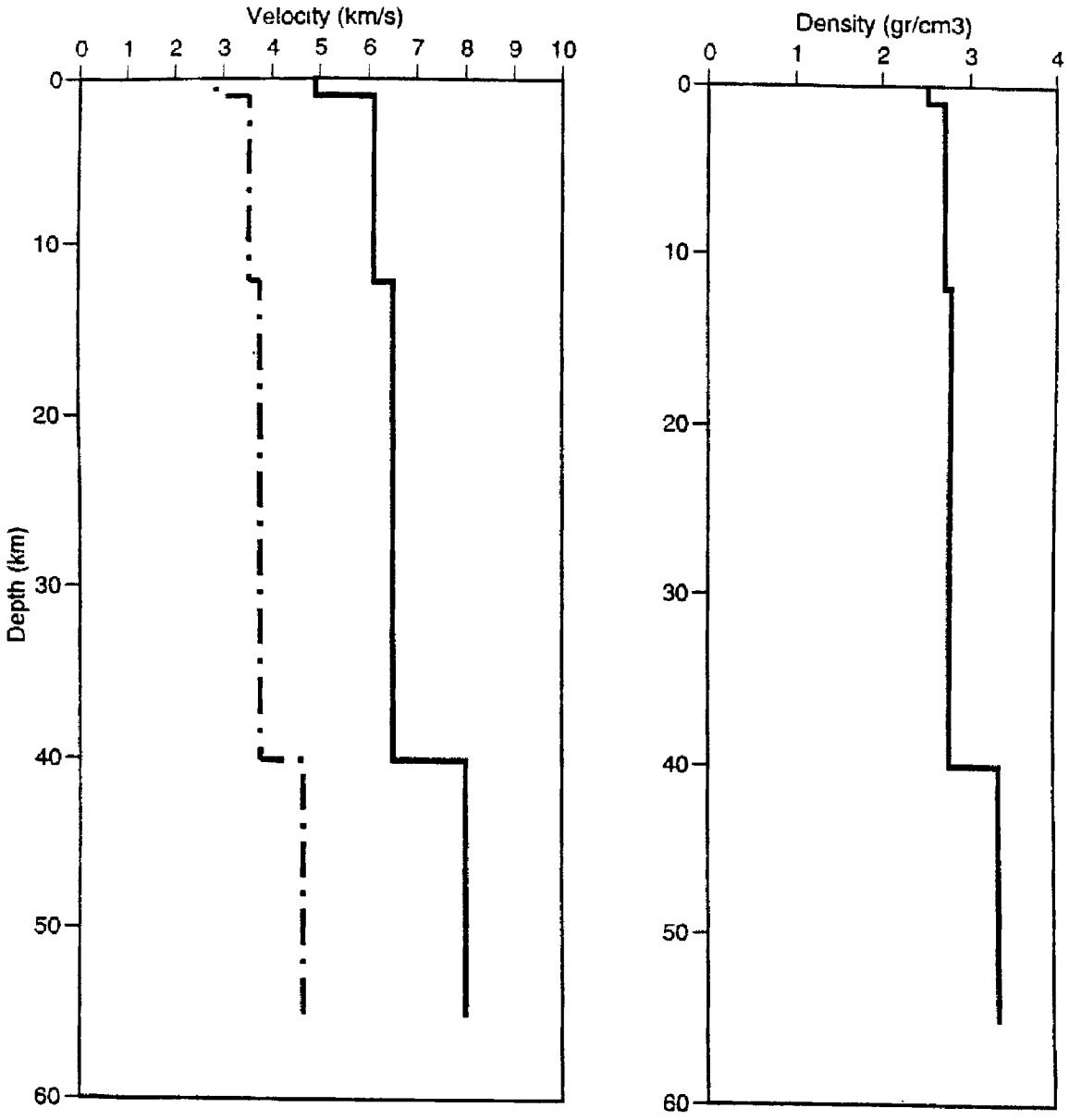

FIGURE 4-1 EPRI Mid-Continent Crustal Model

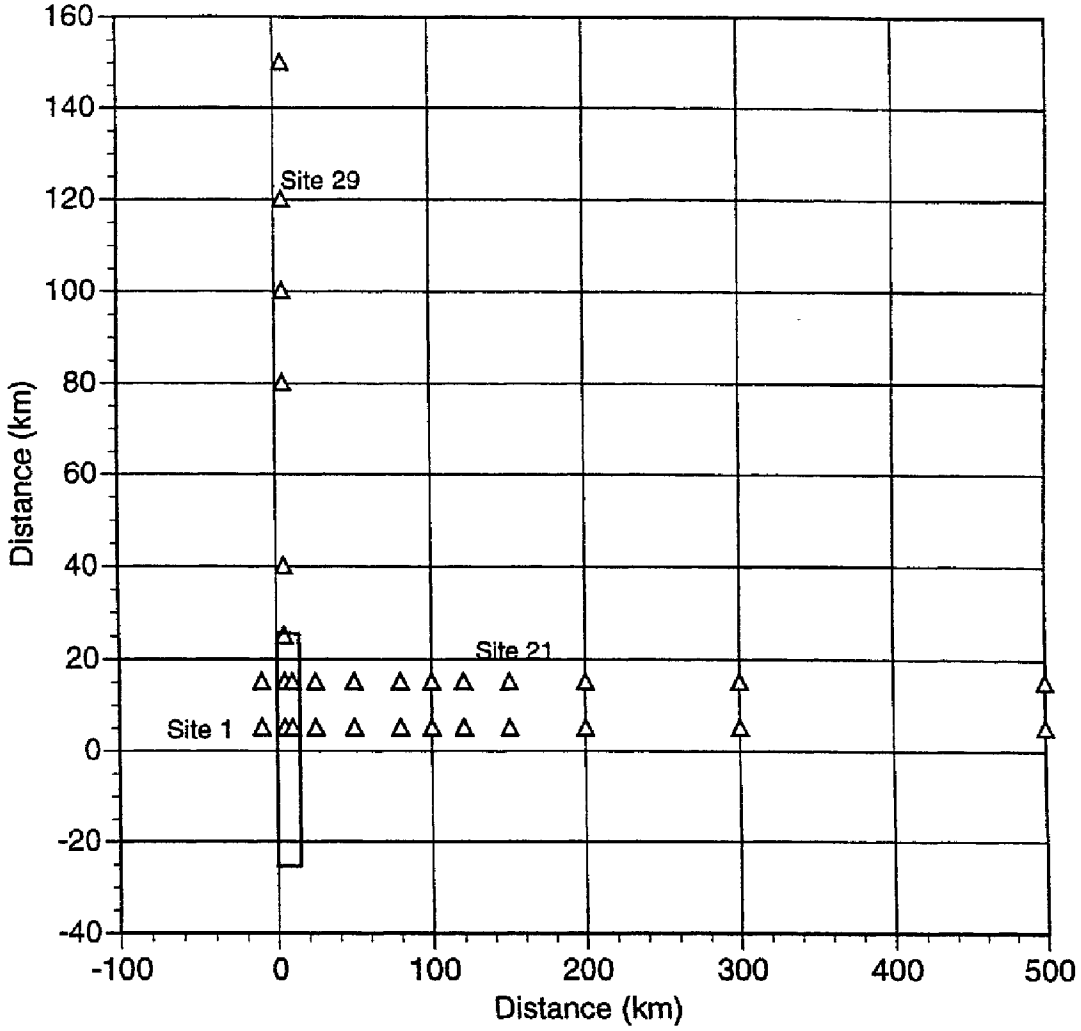

FIGURE 4-2 Simulation Exercise Fault Geometry and Site Locations

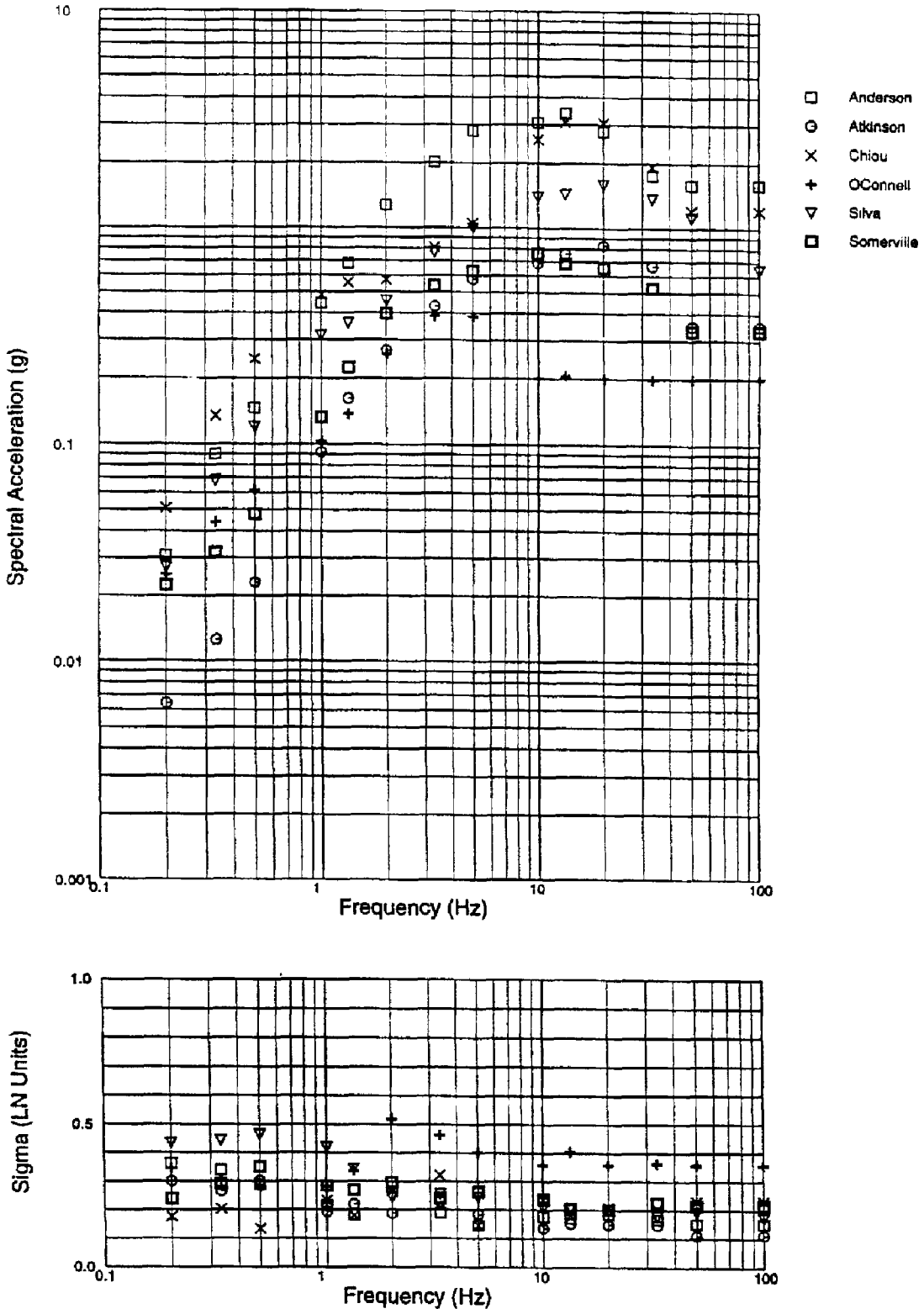

FIGURE 4-3 Scenario Site 1: Spectral Acceleration (5% Damping) and Parametric Variability of Horizontal Ground Motions Computed in Scenario Modeling Exercise (Note: The average spectrum of the two horizontal components is shown.)

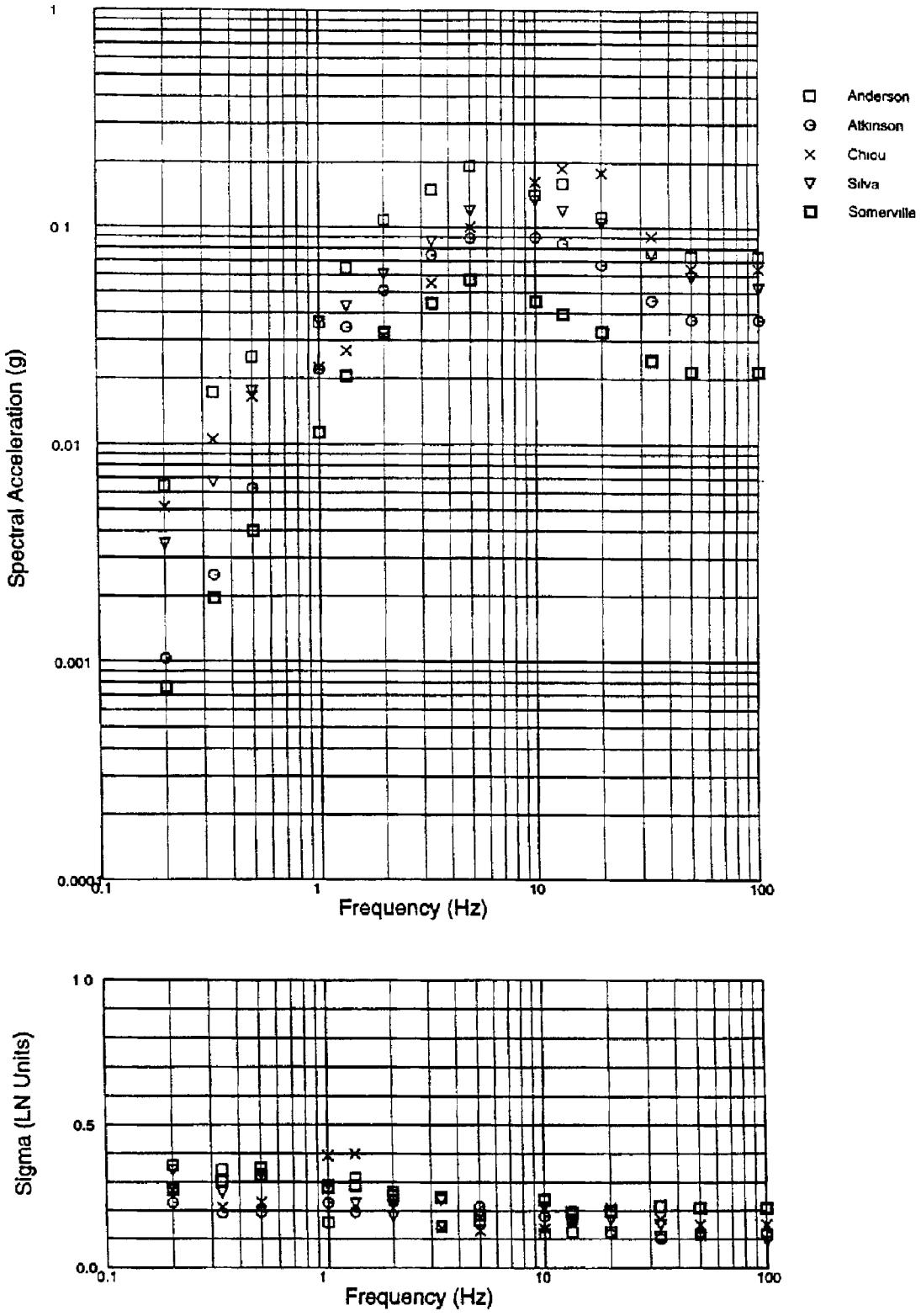

FIGURE 4-4 Scenario Site 21: Spectral Acceleration (5% Damping) and Parametric Variability of Horizontal Ground Motions Computed in Scenario Modeling Exercise (Note: The average spectrum of the two horizontal components is shown.)

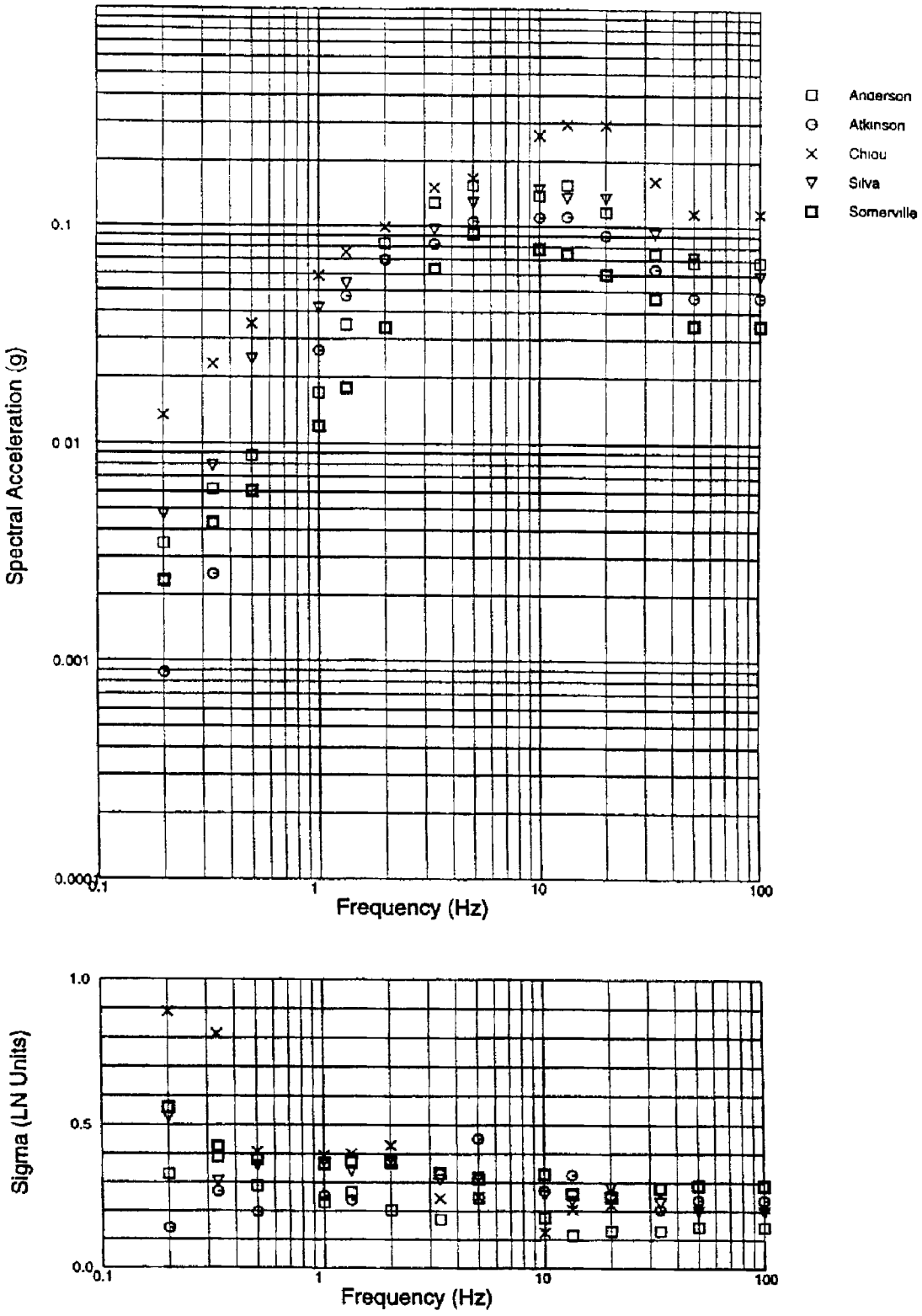

FIGURE 4-5 Scenario Site 29: Spectral Acceleration (5% Damping) and Parametric Variability of Horizontal Ground Motions Computed in Scenario Modeling Exercise (Note: The average spectrum of the two horizontal components is shown.)

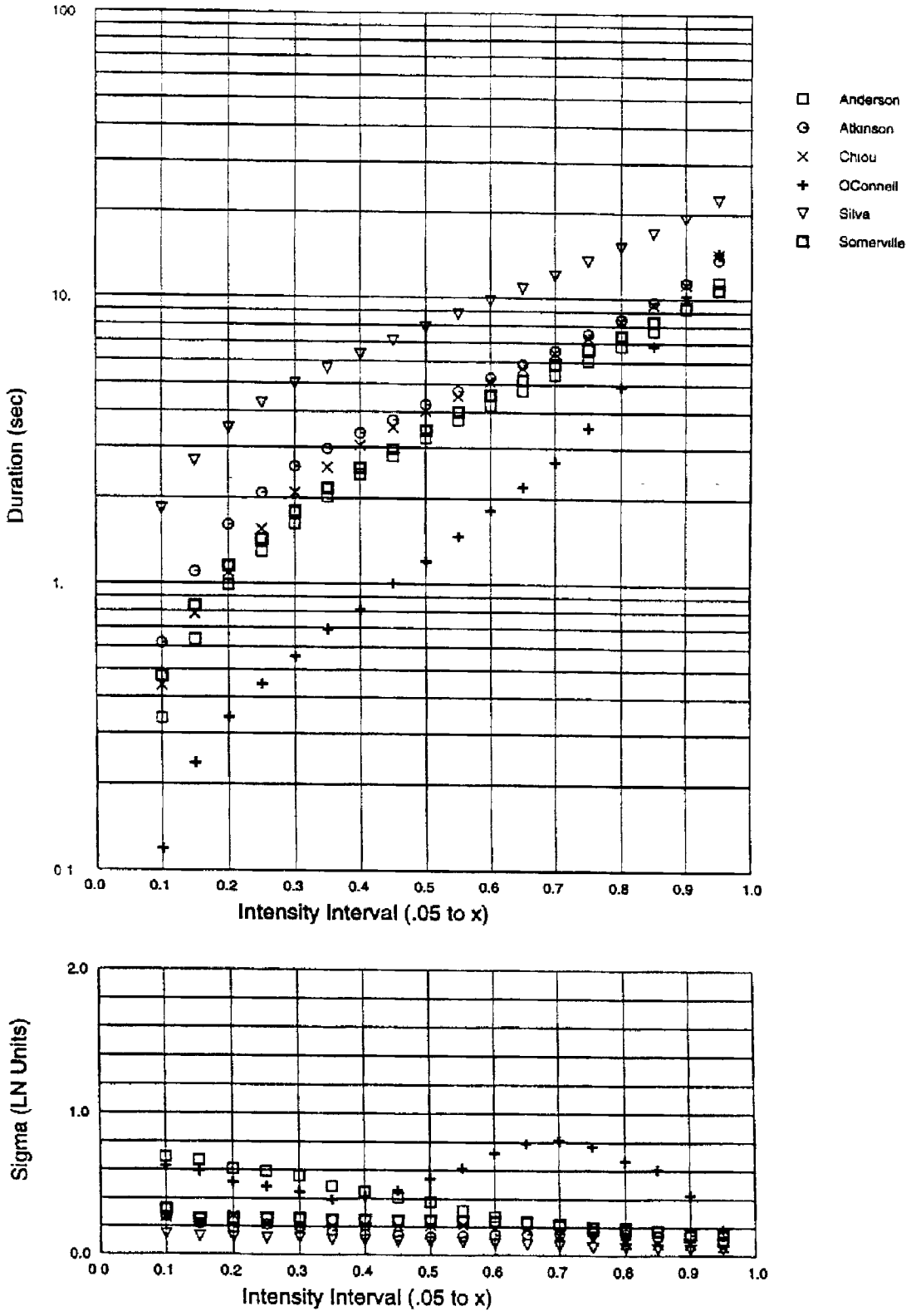

FIGURE 4-6 Scenario Site 1: Acceleration Duration of Horizontal Ground Motions Computed in Scenario Modeling Exercise
(Note: Durations of the average of the two horizontal components are shown.)

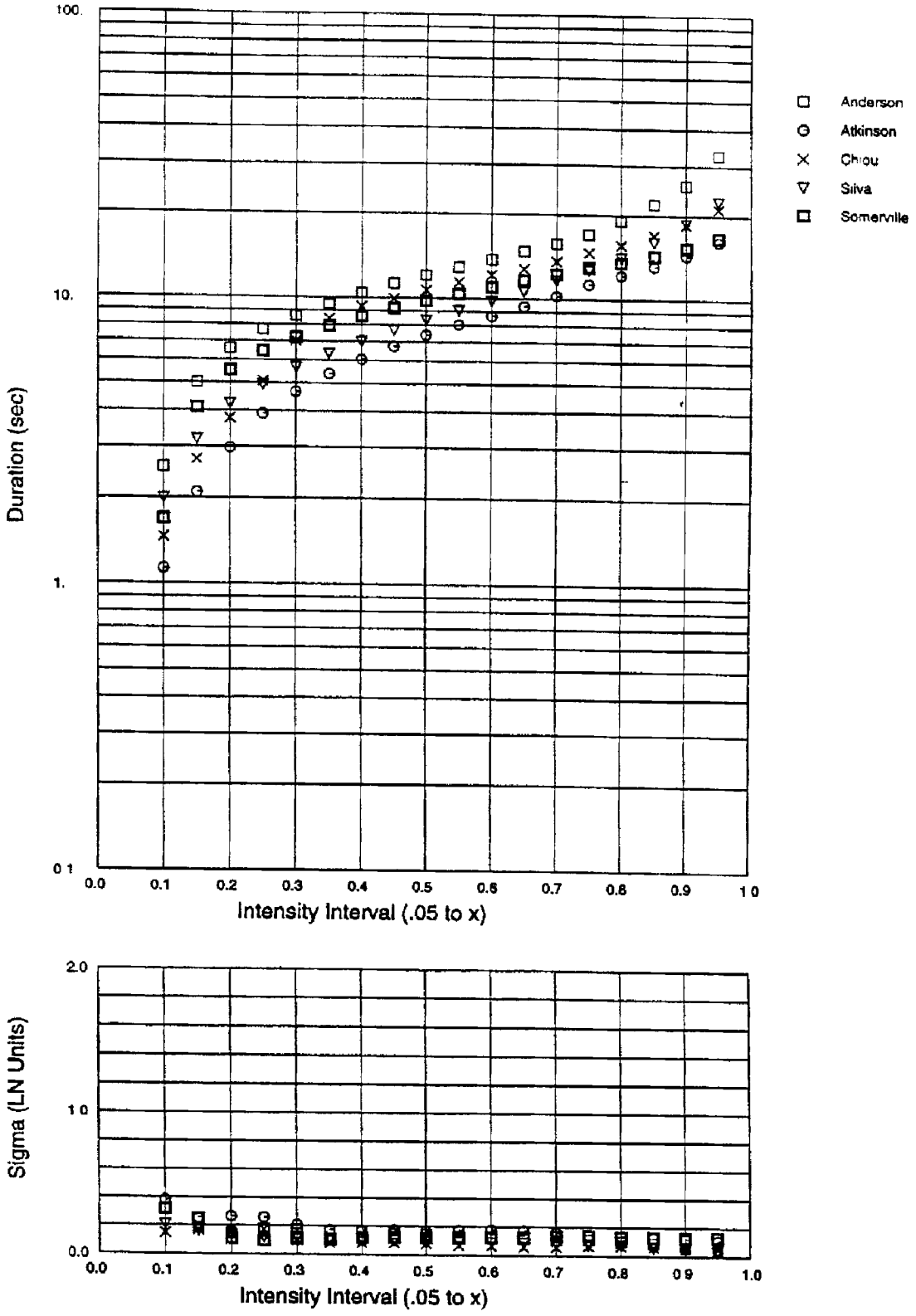

FIGURE 4-7 Scenario Site 21: Acceleration Duration of Horizontal Ground Motions Computed in Scenario Modeling Exercise
(Note: Durations of the average of the two horizontal components are shown.)

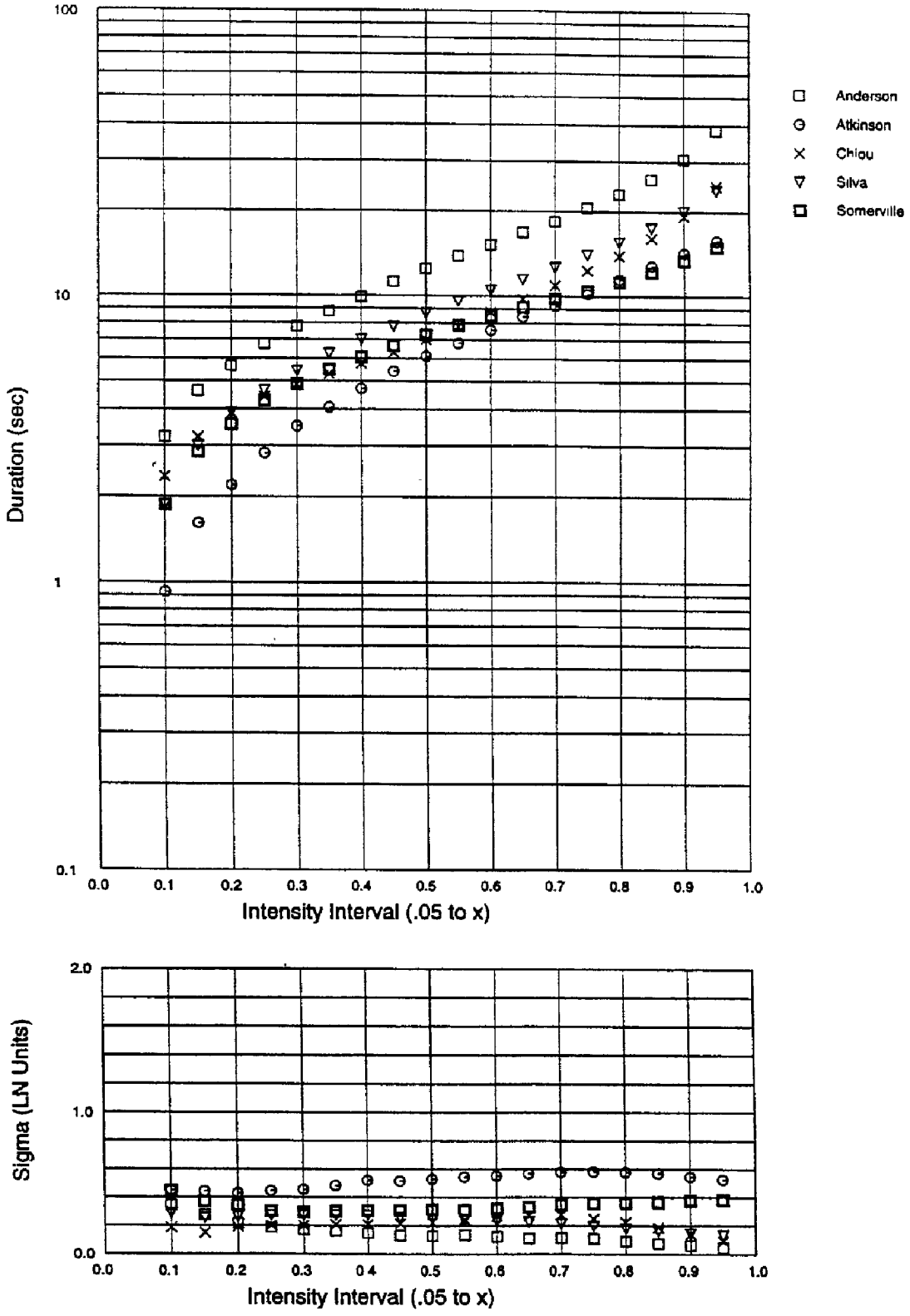

FIGURE 4-8 Scenario Site 29: Acceleration Duration of Horizontal Ground Motions Computed in Scenario Modeling Exercise
(Note: Durations of the average of the two horizontal components are shown.)

SECTION 5
CONCLUSIONS

The root question addressed in the MCEER/FHWA workshop is whether the existing modeling methods may be confidently applied to ENA projects to develop time histories and attenuation relations for engineering analyses. In terms of providing time histories, the methods can produce time histories with reasonable non-stationary characteristics, but they will likely need to be scaled to the design spectral level. Regarding attenuation relations, intuitively, finite fault methods present a better seismological model of the physical process than point source models that are the basis of existing EUS attenuation relations, but additional source parameters required makes these models less robust. Finite fault models will not be ready for use in attenuation relations for ENA until adequate validation is completed. Based on comparisons of the simulated values for all methods, there are differences of up to factors of 5 in amplitude and duration between the different models. There is a wide range in the number of earthquakes against which the methods have been validated - from 1 to 17 earthquakes (Table 3-1). Validation against a standard earthquake data set, with an adequate number of recordings for each earthquake, should significantly reduce this range of model predictions. For example, the range in predictions between those models with more validations varies by about a factor of 3 as compared to a factor of 5 for all the models.

The single-event validation provided an example of the validation process but should not be taken by itself as an evaluation of the models. Some of the models have been shown in other validation exercises to well-match recorded motions on average. A comprehensive series of validations of each model should be performed and thoroughly documented. Taking this to be the case, the workshop provided a valuable forum for proponents of the less well-studied models to begin the validation process.

The variation in simulation results for the models studied is large; however, at high frequencies, the total aleatory variability is larger than the epistemic uncertainty due to different simulation procedures. The epistemic uncertainty and aleatory variability of horizontal spectral acceleration for site 21 lying about 150 km normal to the strike of the fault plane are shown in Figure 5-1. Although the epistemic uncertainty between median ground motions for different methods is much larger than parametric variability within a model, the total aleatory variability (combination of modeling variability and parametric variability) is larger than the epistemic uncertainty. Since the epistemic uncertainty is not dominate except at long periods, this gives some confidence in the use of simulations to predict the distribution of the ground motion for use in engineering applications. Further validations of the methods against a larger data set should help to reduce the epistemic uncertainty.

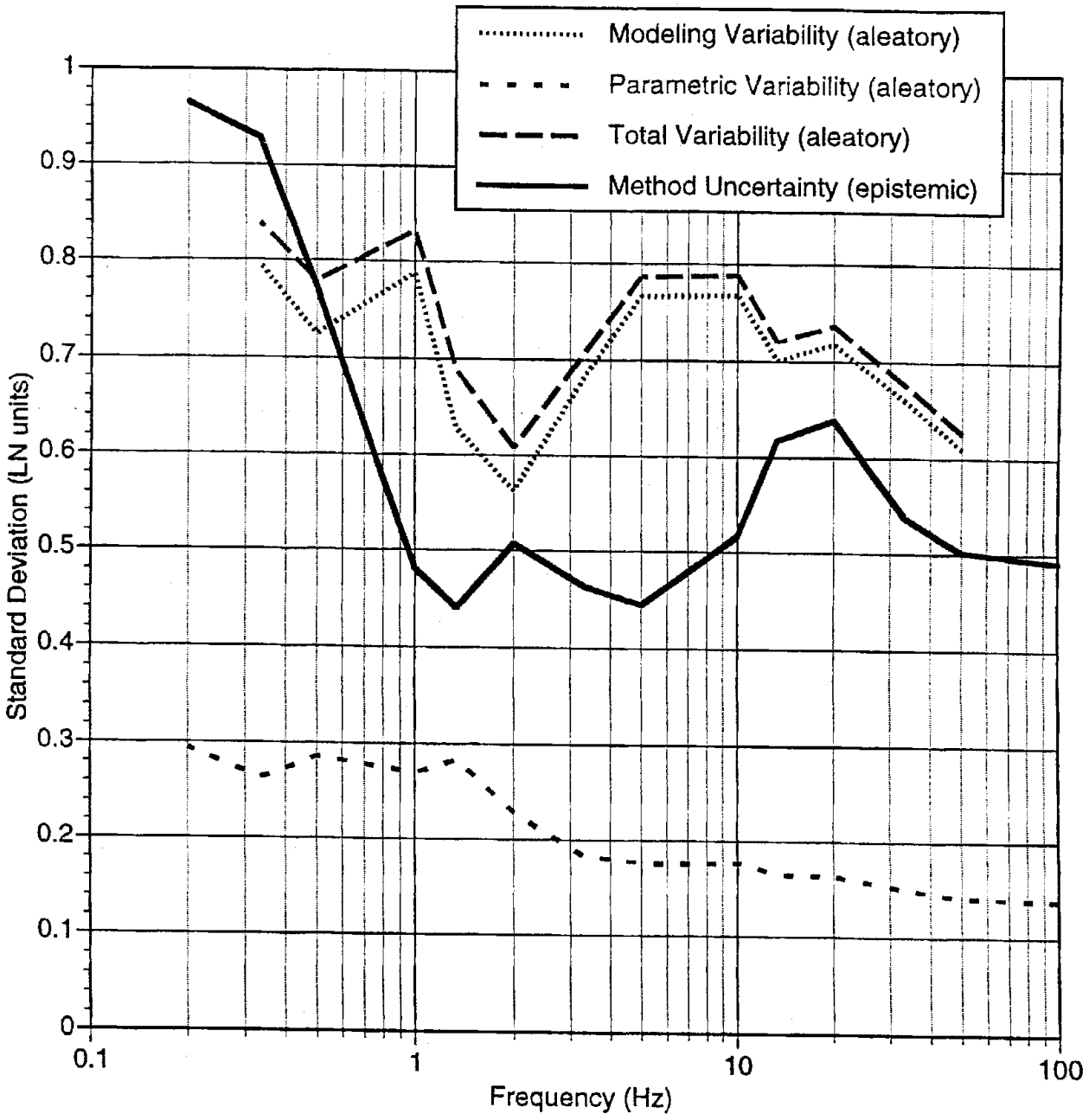

FIGURE 5-1 Comparison of Aleatory Variability and Epistemic Uncertainty Site 21 (Note: At high frequencies, the aleatory variability is larger than the epistemic uncertainty due to the different simulation models.)

The consensus opinion among workshop participants is that model acceptability criteria should be developed which define permissible limits on model bias. Methods that are documented and meet the criteria, using a standard set of validation records archived in a library, could then be objectively identified as adequate for application in the EUS. Participants agreed the validation library should include strong motions from all ENA earthquakes with magnitude greater than 4.5, regardless of recording distance. About ten WUS events should also be included, with magnitudes greater than about 5.5 and motions recorded at distances of less than 100 km.

This type of comprehensive model validation process presents a large task for modelers, but it is a necessary step. Until this is done, unacceptably large differences in simulated ground motions between different modelers will remain.

SECTION 6
REFERENCES

Beresnev, I.A., and G.M. Atkinson (1997), "Modeling Finite-Fault Radiation from the ω^n Spectrum," *Bull. Seism. Soc. Am.*, 87, 67-84.

Beresnev, I.A. and G.M. Atkinson (1998a), "FINSIM - A FORTRAN Program for Simulating Stochastic Acceleration Time Histories from Finite Faults," *Seism. Res. Lett.*, 69, 27-32.

Beresnev, I.A. and G.M. Atkinson (1998b), "Stochastic Finite-Fault Modeling of Ground Motions from the 1994 Northridge, California Earthquake, I, Validation on Rock Sites," *Bull. Seism. Soc. Am.* (in review).

Beresnev, I.A. and G.M. Atkinson (1998c), "Generic Finite-Fault Model for Ground-Motion Prediction in Eastern North America," submitted to *Bull. Seism. Soc. Am.*

Bernard, P., Herrero, A. and C. Berge (1996), "Modeling Directivity of Heterogeneous Earthquake Ruptures," *Bull. Seism. Soc. Am.*, 86, 1149-1160.

Boatwright, J. and G. Choy (1992), "Acceleration Source Spectra for Large Earthquakes in Northeastern North America," *Bull. Seism. Soc. Am.*, 82, 660-682.

Boore, D.M. (1983), "Stochastic Simulation of High-Frequency Ground Motions Based on Seismological Models of the Radiated Spectra," *Bull. Seism. Soc. Am.*, 73, 1865-1894.

Boore, David M. and Gail M. Atkinson (1992), "Source Spectra for the 1988 Saguenay, Quebec, Earthquakes," *Bull. Seism. Soc. Am.*, 82, 683-719.

Frankel, A. (1991), "High-Frequency Spectral Fall-off for Earthquakes, Fractal Dimension of Complex Rupture, B-value, and the Scaling of Strength on Faults," *J. Geophys. Res.*, 96, 6291-6302.

Haddon, R.A.W. (1992), "Waveform Modeling of Strong-Motion Data for the Saguenay Earthquake of 25 November 1988," *Bull. Seism. Soc. Am.*, 82, 720-754.

Hartzell, S., Langer, C. and C. Mendoza (1994), "Rupture Histories of Eastern North American Earthquakes," *Bull. Seism. Soc. Am.*, 84, 1703-1027.

Herrero, A. and P. Bernard (1994), "A Kinematic Self-Similar Rupture Process for Earthquakes," *Bull. Seism. Soc. Am.*, 83, 1216-1228.

Hutchings, L.J. and F. Wu (1990), "Empirical Green's Functions from Small Earthquakes - A Waveform Study of Locally Recorded Aftershocks of the San Fernando Earthquake," *J. Geophys. Res.*, 95, 1187-1214.

Hutchings, Lawrence (1991), "'Predictions' of Small Ground Motion for the 1989 Loma Prieta Earthquake Using Empirical Green's Functions," *Bull. Seism. Soc. Am.*, 81, 1813-1837.

Hutchings, Lawrence (1994), "Kinematic Earthquake Models and Synthensized Ground Motion Using Empirical Green's Functions," *Bull. Seism. Soc. Am.*, 84, 1028-1050.

Jarpe, S.P. and P.W. Kasameyer (1996), "Validation of a Procedure for Calculating Broadband Strong-Motion Time Histories with Empirical Green's Functions," *Bull. Seism. Soc. Am.*, 86, 1116-1129.

Joyner, W.B. (1995), "Stochastic Simulation of Near-Source Earthquake Ground Motion," *Proceedings of Workshop on Modeling Earthquake Ground Motion at Close Distances*, September 5-6, 1990, EPRI Report EPRI TR-104975.

Luco, J.E. and R.J. Apsel (1983), "On the Green's Functions for a Layered Half Space, Part 1," *Bull. Seism. Soc. Am.*, 73, 909-929.

Silva, W.J. and K. Lee (1987), "WES RASCAL Code for Synthesizing Earthquake Ground Motions," *State of the Art for Assessing Earthquake Hazards in the United States*, Report 24, U.S. Army Waterways Experiment Station, Misc. Paper S-73-1.

Somerville, P.G., McLaren, J.P., Saikia, C.K. and D.V. Helmberger (1990), "The 25 November 1988, Quebec, Earthquake: Source Parameters and the Attenuation of Strong Ground Motion," *Bull. Seism. Soc. Am.*, 80, 1118-1143.

Somerville, P.G. (1993), "Engineering Applications of Strong Ground Motion Simulation," *Tectonophysics*, 218, 195-219.

Su, Feng, Anderson, John G., Brune, James N. and Yuehua Zeng (1996), "A Comparison of Direct S-Wave and Coda Wave Site Amplification Determined from Aftershocks of the Little Skull Mountain Earthquake," submitted for publication to *Bull. Seism. Soc. Am.*, Feb. 5.

Zeng, Y. and J.G. Anderson (1994), "A Method for Direct Computation of the Differential Seismogram with Respect to the Velocity Change in a Layered Elastic Solid," *Bull. Seism. Soc. Am.*, 73, 909-929.

Zeng, Y., Anderson, J.G. and F. Su (1995), "Subevent Rake and Random Scattering Effects in Realistic Strong Ground Motion Simulation," *Geophys. Res. Lett.*, 22, 17-20.

Zeng, Y., Anderson, J.G. and G. Yu (1994), "A Composite Source Model for Computing Realistic Synthetic Strong Ground Motions," *Geophys. Res. Lett.,* 21, 725-728.